Responses to reviewer #1

We thank the reviewer for these comments that have help us to improve the overall quality of the paper. We apologize for an inconvenient way of providing answers in the previous review cycle. In what follows, after each reviewer comment (in black) our response is in blue and the revised manuscript text in bold blue.

In end the of this document we list changes in figures numbering.

Page2, Line 5: I suggested citing these papers (Hausmann and Platt, 1994; Simpson et al., 2007; Abbatt et al., 2012) when discussing tropospheric BrO, not stratospheric ozone depletion. These papers are not appropriate references here.
We moved (Hausmann and Platt, 1994; Simpson et al., 2007; Abbatt et al., 2012) to the their relevant location when discussing previous tropospheric BrO studies. The new text reads as follows:

Bromine monoxide (BrO) is a halogen oxide, predominantly located in the stratosphere and upper troposphere where, like chlorine monoxide (ClO), it is a catalytic element in the destruction of stratospheric ozone (von Glasow *et al.*, 2004; Salawitch *et al.*, 2005), but with higher efficiency per molecule. Sources of tropospheric BrO include bromine release ("explosions") during the Polar Spring (Hausmann and Platt, 1994; Hollwedel *et al.*, 2004; Simpson *et al.*, 2007; Begoin *et al.*, 2010; Salawitch *et al.*, 2010; Abbatt, *et al.*, 2012; Blechschmidt *et al.*, 2016), volcanic eruptions (Bobrowski *et al.*, 2003; Chance, 2006; Theys *et al.*, 2009;), salt lakes (Hebestreit, *et al.*, 1999; Hörmann *et al.* 2016) and stratospheric transport (Salawitch *et al.*, 2010).

Page 7, Line 21: I don't think the other reviewer was out of line asking for more detail on the fitting window selection here. The other reviewer's concerns about the choice of fitting window should be addressed by the addition of a more detailed description of how the authors arrived at this choice of fitting window. I certainly do not agree with the sentiment expressed by the authors that the other reviewer's arguments should be discounted. The onus is on the author to convince the reviewer/editor to accept their paper. How is one supposed to believe that "The update of the BrO fitting window from V2 to V3 in 2011 is not arbitrary, but is based on substantial quantitative analysis by checking the quality of BrO retrievals and the correlation with other trace gases while systematically varying the lower and upper limits of fitting windows, similar to the studies of Chan Miller et al. (2014)." if these analyses are not detailed or described in the manuscript? The fact that the authors "were then the first to fit BrO from GOME-1 and have fitted BrO from SCIAMACHY, OMI, and OMPS" does not excuse them from responding to legitimate concerns about the quality of their work, particularly when trying to publish said work in a peer reviewed journal.

The selection of the new fitting window was based on extended sensitivity analysis aiming at reducing fitting uncertainties and retrieval noise while keeping algorithm stability. We have modified the text in section 3.2 to include this explanation:

"For improved numerical stability, radiances and irradiances are divided by their respective averages over the fitting window, renormalizing them to values of ~1. BrO is fitted in the spectral window 319.0–347.5 nm, within the UV-2 channel of the OMI instrument. The switch from the previous fitting window of 340–357.5 nm to the wider new one using shorter wavelengths is based on extensive sensitivity analysis. This new fitting window aims at reducing the fitting uncertainty by including more BrO spectral structures as shown in Fig. 1 and reducing retrieval noise while preserving the stability of the algorithm. An analysis of the retrieval sensitivity to different windows is included in section 3.5."

Section 3.5 in the paper discusses error sources. It includes table #1 where we have included results from the sensitivity runs performed with different fitting windows. We are not including here the text of the new section in lieu of brevity. The fitting windows tested include: 340–357.5 (previous version fitting window), 323-353, 327-359, 332-359 and 337-359 nm.

Changes in figures numbering

Old manuscript	Updated manuscript
Figure 1	Figure 1
Figure 2	Figure 2
Figure 3	Figure 3
----	Figure 4 is a new figure
Figure 4	Figure 5
Figure 5	Figure 6
----	Figure 7 is a new figure
Figure 6	Figure 8
Figure 7	Figure 9
---	Figure 10 is a new figure
Figure 8	Figure 11
Figure 9	Figure 12
Figure 10	Figure 13
Figure 11	Figure 14

Responses to reviewer #2:

Authors of the paper "OMI total bromine monoxide (OMBRO) data product: Algorithm, retrieval and measurement comparisons" put quite some effort into addressing the Referees' comments. Especially the presentation of the comparison to GOME-2 and ground-based data has been improved significantly. Some parts of the paper were successfully restructured, but I still miss substantial information about the presented algorithm. I am furthermore disappointed that my previous comments have not been treated thoroughly enough as detailed below.

We will like to thank the reviewer for the thoughtful comments that are helping us to improve the overall quality of the paper. In what follows, our responses are typed using blue. Any text that has been added or modified in the manuscript and is included in these responses is typed in bold blue. We hope that the answers we provide for the remaining questions are satisfactory and once more we will like to thank the reviewer for the time and efforts put in providing constructive feedback.

In end the of this document we list changes in figures numbering.

Besides that, I could not find a rationale for adding the Dead Sea Valley data in the responses. It has certainly not been requested by the Referees. I would like to communicate my concerns towards this sudden extension. (1) Instead of improving the quality for the original study (e.g. study influence of clouds, albedo) at the Great Salt Lake, another study featuring similar shortcomings was added. (2) In any way, I would have expected the authors to set their findings into relation with existing observations of the same area as published by Hörmann et al. (2016).

Attending the reviewer comments we have decided to remove the Dead Sea Valley plot in the re-submitted paper. We have modified figure 9 to show the cloud properties and the albedo. We have also decide to show data for June 2006. Given the SZA, June is a more favorable month for observations at the Great Salt Lake and in 2006 OMI was not affected by the row anomaly. Now these section reads as:

"Following recent work by Hörmann et al. (2016) over the Rann of Kutch we have explored the capability of OMBRO to observe similar enhancements in other salt lakes. Fig. 12 shows monthly averaged OMI BrO over the Great Salt Lake for 06/2006, the corresponding surface albedo used in the retrieval, cloud cover (after filtering out pixels with cloud cover bigger than 40%) as well as the cloud pressure. Over the Great Salt Lake, BrO enhancement occurs predominantly over the lake bed with enhancements of ~5-10×10^{12} molecules cm^{-2} over background values (3-4×10^{13} molecules cm^{-2}). Despite observing these enhancements, the users of OMBRO should be aware of three limitations of the current retrieval algorithm for this kind of studies. First, the BrO columns assume a mostly stratospheric BrO profile (Figure 3) for the AMF calculation. Second, the OMI derived albedo climatology (Kleipool *et al.* 2008) used in OMBRO has a resolution of 0.5 degrees. At this resolution OMBRO retrievals can have biases given the size of OMI pixels and the inherent sub-pixel albedo variability. Finally, high surface albedos inherent to salt lakes yield abnormally high cloud fractions and low clouds over the salt lakes (Hörmann *et*

_al_., 2016). All these factors should be considered in studies addressing the spatiotemporal distribution of BrO over salt lakes using OMBRO."

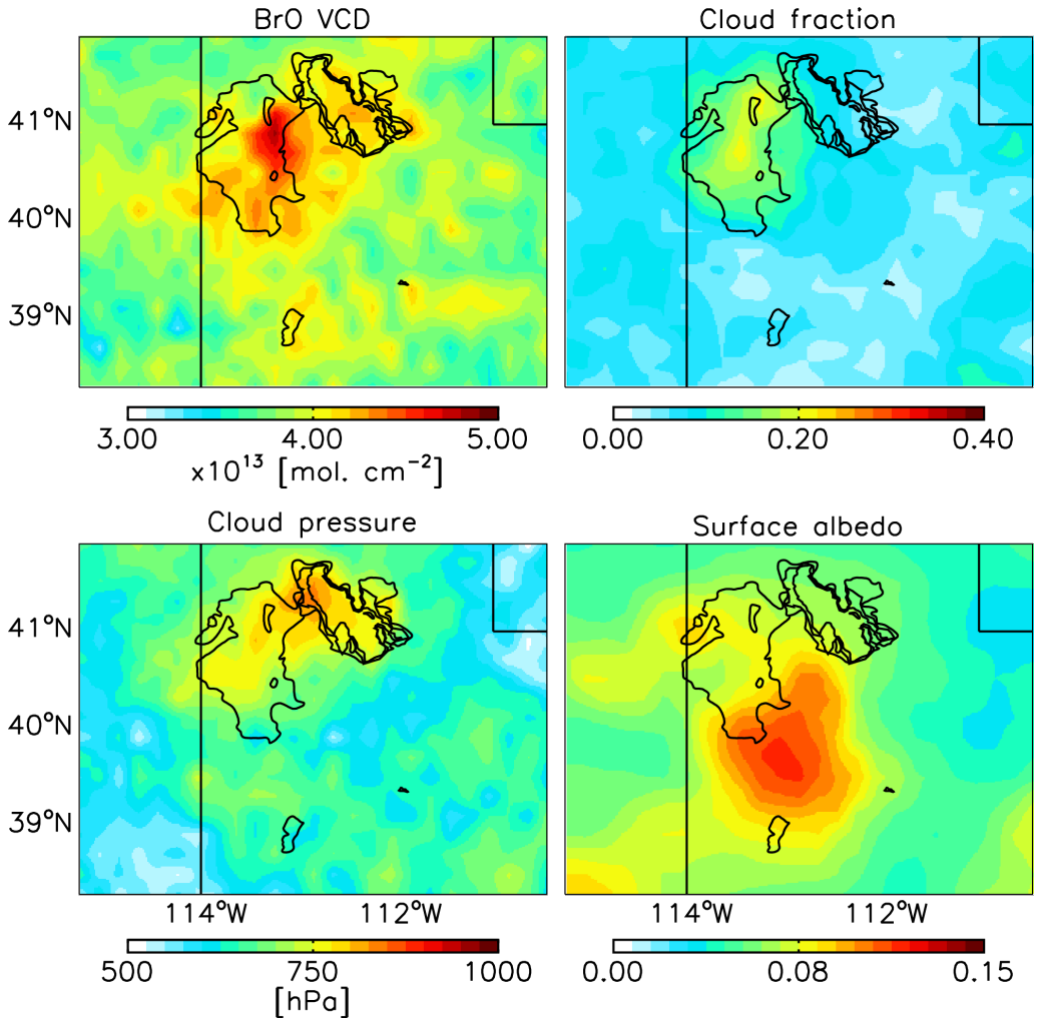

Figure 12. Mean June 2006 BrO VCD, cloud fraction, cloud pressure and surface albedo over the Great Salt Lake area. Averages have been calculated on a 0.2 x 0.2 degree grid including only pixels with cloud fractions smaller than 0.4.

In the following I am going to comment on some of the Author Responses. Original Referee Comments are denoted with >>, Authors Responses by >, and my comments with leading -->.

>> The least the authors could have done would be to include a plot showing results using the "Traditional" and "OMI current" wavelength ranges.

--> This advice has been addressed neither in the responses nor in the manuscript.

> The update of the BrO fitting window from V2 to V3 in 2011 is not arbitrary, but is based on substantial quantitative analysis by checking the quality of BrO retrievals and the correlation

with other trace gases while systematically varying the lower and upper limits of fitting windows, similar to the studies of Chan Miller et al. (2014).

--> In my original comments I expressed my concerns against the choice of the “new fitting window”. I now really wonder how the results of the claimed “substantial quantitative analysis” look like. Why are they not presented to convince the actual reader of the article? Vogel et al. (2013), which I am still missing in the references, presented such a study for BrO while the cited Chan Miller et al. (2014) performed such a study on Glyoxal, whose constrains are quite different. I suggest to include the results of such tests for OMBRO in a future version of this manuscript.

We include here a picture showing the results of the algorithm for one orbit using the current operational fitting window (V3) (top panel), the fitting window of V1 (middle panel), and the fitting window of V2 (lower panel). The reduced noise levels in the retrieval using the new fitting window are apparent. More specifically retrieval noise levels of V2.01 fitting window are on the order of 1.29×10^{13} molecules cm^{-2}, on the order of 1.01×10^{13} molecules cm^{-2} for V3.02 while using V3.09 fitting windows those are reduced to 7.85×10^{12} molecules cm^{-2}.

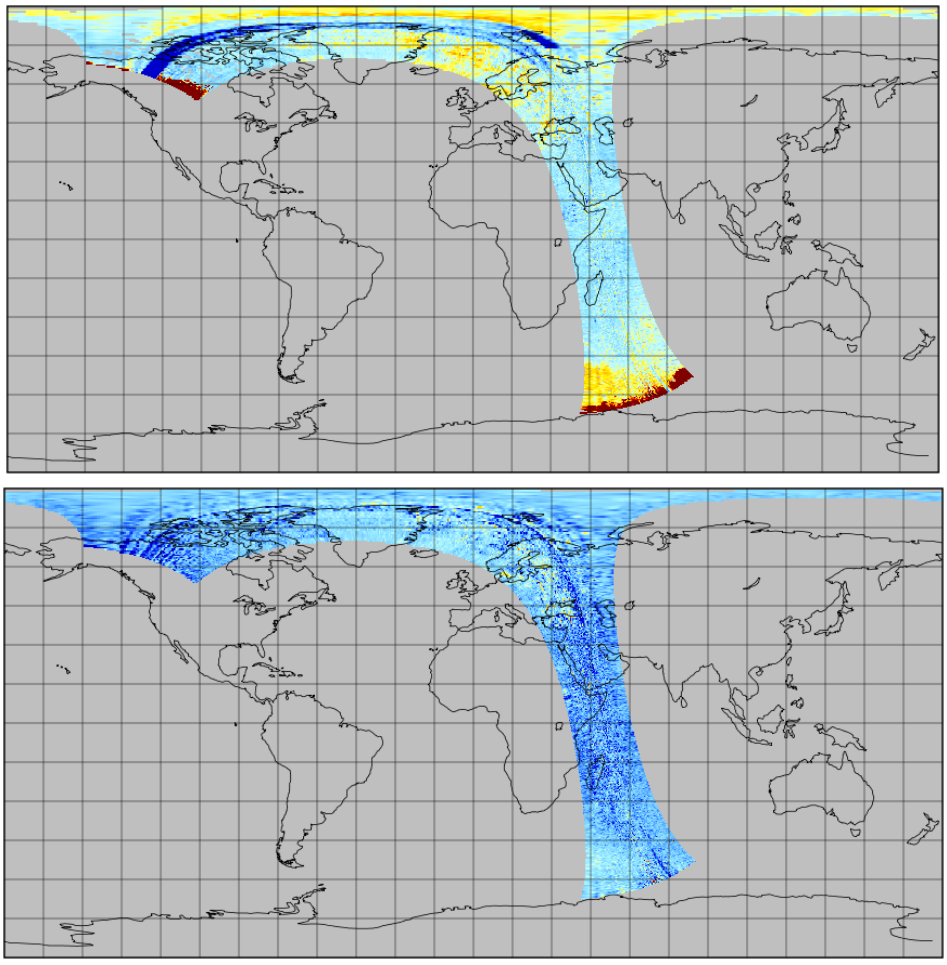

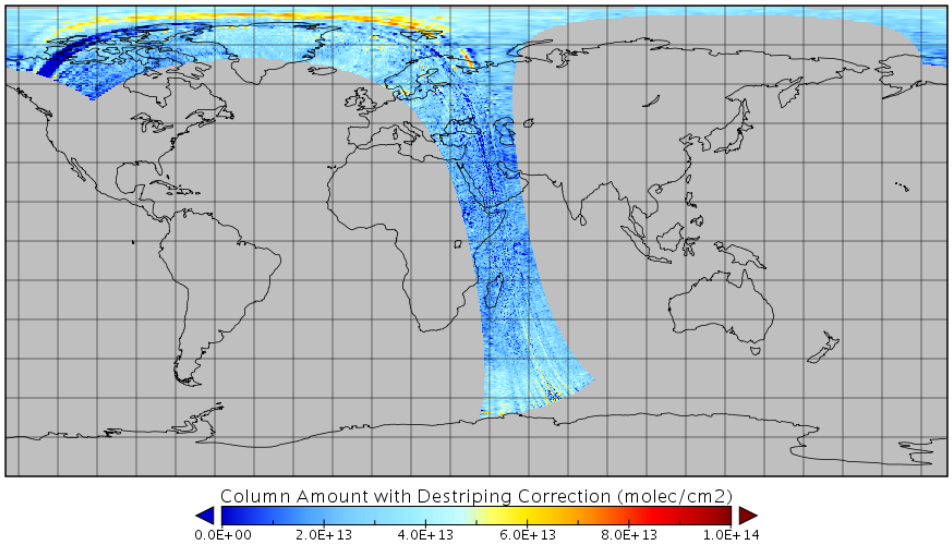

We have also included a fitting window sensitivity analysis in section 3.5 reporting error estimates. See answer to reviewer #3 and updated manuscript for further details. We added Vogel et al., 2013 to the references and to the manuscript.

>> - Please add (Liao et al., 2011) and (Frieß et al., 2012) to the references for Barrow, Alaska since both papers present significant BrO observations of near-surface BrO.

> The recommended two references were added. Please note that Liao, et al., 2011 was finally published in 2012 and Frieß was published in 2011 not 2012.

--> The authors are correct about my mistake about the Freiß et al. paper. However, the Liao paper they decided to include in the manuscript is not the one I recommended. I provided a correct reference to Liao et al. (2011) with double-checked DOI (10.1029/2010jd014788), which has not been interpreted correctly.
We added the correct Liao et al. (2011) paper. Please see Page 23, Line 4-10.

> Toyota et al. (2011) is a modeling paper and it has no observations or comparison to any satellite or ground-based measurements, so it is not added.

--> This is not correct. If the authors would have taken the time to open the correctly provided reference with double-checked DOI (10.5194/acp-11-3949-2011) - an open access paper - they would have found comparisons between model and ground-based measurements in Figs. 3, 4, and 5. Comparisons between model and satellite data are shown in Fig. 8. Please add this reference.
We added the Toyota et al. (2011) paper. Please see Page 29, Line 1-3 and the introduction text: **"Global BrO measurements from space were first proposed for the Scanning Imaging Absorption Spectrometer for Atmospheric Cartography (SCIAMACHY) instrument (Chance *et al.*, 1991) and were first demonstrated with Global Ozone Monitoring Experiment (GOME-1) measurements (Chance, 1998; Platt and Wagner, 1998; Richter *et***

***al*., 1998), and since with SCIAMACHY nadir (Kühl *et al*., 2008) and Global Ozone Monitoring Experiment 2 (GOME-2) measurements (Theys *et al*., 2011; Toyota *et al*., 2011)."**

> We also raise attention to the fact that abnormally high cloud fractions are reported over the salt lakes due to enhanced albedos. All these considerations are important for future studies studying spatiotemporal distribution of BrO over salt lakes.

--> I am missing a reference to Hörmann et al. 2016, who actually included the issue (clouds and albedo) into their study. Not only "future studies" need to take care of this, but past studies already did, which should be acknowledged here.
Our answer to the first comment addresses this question (see above).

>> e) Fig. 10: This plot does not allow an independent judgment whether this is a significant signal or not. Suggested improvements:
- Increase area significantly
- Use full colorscale
- Thicker coast lines
- Align with other geospatial properties: cloud statistics, albedo, precipitation etc.

> Response:
Old Figure 10 (now Figure 9) has been updated: We increased the covered area, used full color scale, and added the lake line. We also added another panel to show BrO enhancement over the Dead Sea Valley for September 2007.

--> I am not convinced by the updated figure. The comments suggested to add auxiliary geospatial information in order to increase confidence in the reported enhancement over the Great Salt Lake similar to the study performed by Hörmann et al., 2016. This suggestion has been ignored.
Our answer to the first comment addresses this question (see above).

> Response:
Yes. The text was moved to the Introduction (see Page 3 Line 4-11) and was changed to **"Enhancement of BrO in the vicinity of salt lakes like the Dead Sea and the Great Salt Lake have been observed from ground-based measurements (Hebestreit et al., 1999; Matveev et al., 2001; Stutz et al., 2002; Tas et al., 2005; Holla et al., 2015). The active bromine compound release is due to the reaction between atmospheric oxidants with salt reservoirs. Satellite observation of salt lake BrO was first reported over the Great Salt Lake and the Dead Sea from OMI (Chance, 2006; Hörmann et al. 2016). Seasonal variations of tropospheric BrO over the Rann of Kutch salt marsh have been observed using OMI from an independent research BrO product (Hörmann et al. 2016)."**

--> Please add that also Hörmann et al., 2016 reported on the detection of BrO in the Dead Sea Valley using OMI observations. Chance (2006) might have been the first one, but the text may

suggest that Hörmann et al. (2016) reported only on the BrO enhancements over the Rann of Kutch.
Hörmann et al., 2016 has been added. Please see Page 3, Line 6.

New References

Hörmann, C., Sihler, H., Beirle, S., Penning de Vries, M., Platt, U., and Wagner, T.: Seasonal variation of tropospheric bromine monoxide over the Rann of Kutch salt marsh seen from space, Atmos. Chem. Phys., 16, 13015-13034, doi:10.5194/acp-16-13015-2016, 2016.

K. Toyota, J. C. McConnell, A. Lupu, L. Neary, C. A. McLinden, A. Richter, R. Kwok, K. Semeniuk, J. W. Kaminski, S.-L. Gong, J. Jarosz, M. P. Chipperfield, and C. E. Sioris, Atmos. Chem. Phys., 11, 3949-3979, doi:10.5194/acp-11-3949-2011, 2011.

J. Liao, H. Sihler, L. G. Huey, J. A. Neuman, D. J. Tanner, U. Friess, U. Platt, F. M. Flocke, J. J. Orlando, P. B. Shepson, H. J. Beine, A. J. Weinheimer, S. J. Sjostedt, J. B. Nowak, D. J. Knapp, R. M. Staebler, W. Zheng, R. Sander, S. R. Hall, and K. Ullmann: A comparison of Arctic BrO measurements by chemical ionization mass spectrometry and long path-differential optical absorption spectroscopy, J. Geophys. Res.-Atmos., 116, D00r02, doi:10.1029/2010jd014788, 2011.

L. Vogel, H. Sihler, J. Lampel, T. Wagner, and U. Platt: Retrieval interval mapping: a tool to visualize the impact of the spectral retrieval range on differential optical absorption spectroscopy evaluations, Atmos. Meas. Tech., 6, 275-299, doi:10.5194/amt-6-275-2013, 2013.

Changes in figures numbering

Old manuscript	Updated manuscript
Figure 1	Figure 1
Figure 2	Figure 2
Figure 3	Figure 3
----	Figure 4 is a new figure
Figure 4	Figure 5
Figure 5	Figure 6
----	Figure 7 is a new figure
Figure 6	Figure 8
Figure 7	Figure 9
---	Figure 10 is a new figure
Figure 8	Figure 11
Figure 9	Figure 12
Figure 10	Figure 13
Figure 11	Figure 14

Responses to reviewer #3:

The manuscript 'OMI total bromine monoxide (OMBRO) data product: Algorithm, retrieval and measurement comparisons' describes the status of the operation OMBRO data product, which provides BrO VCDs retrived from OMI data. Comparisons to ground-based observations and other satellite observations are presented and small case studies for salt-lakes are shown. The global distribution of VCDs is qualitatively compared and found to be similar to those of GOME-2. The data product was found to have problems in case of volcanic eruptions due to interferences due to a sub-optimal choice of the SO2 absorption cross-section.

The manuscript fits perfectly the scope of AMT and should be published for two reasons: Once to have a solid reference for the spectral retrieval settings for satellite retrieved BrO VCDs and also to provide a good reference for end users of the OMBRO dataset. The end users finally need to know the errors which are already introduced by approximations in the spectral retrieval and the conversion to trace gas VCDs in order to estimate the significance of their findings. Typical end-users cannot estimate the importance of different fit parameters of the data product as already pointed out by referee No. 3. A lot of points have been already presented by the two other reviewers, therefore I'll try to keep this short. In my opinion a publication should represent the current state of the art of the respective topic. I understand the limits of the operational data products and I know that such a dataset cannot be reprocessed within short time. However, a publication could list quantitatively uncertainties and also shortcomings of the current data processing. By doing this there would be no need for reprocessing the whole data set (at least for this publication) while providing the end user with the necessary error analysis and already paving the way towards a better and improved data product. This way, the manuscript would be also helpful for other scientists working on the retrieval of weak trace gases in this spectral region from satellite observations.

For the current manuscript however, I don't see that this is the case here, and I furthermore do not see substantial improvement towards this direction from the initial to the revised manuscript.

We will like to thank the reviewer for his detailed comments. We hope that by answering them the quality of the manuscript has been improved. In what follows our answers are typed in blue after the reviewer comment each one of them is addressing is copied in black. If reference is made to the manuscript text this is typed in bold blue.

In end the of this document we list changes in figures numbering.

Major points:

1. The absorption of the oxygen collision complex (short: O4) is not included in the spectral fit settings (c.f. e.g. [Greenblatt et al., 1990, Hermans et al., 1999, Thalman and Volkamer, 2013]. These are used also in [Richard et al., 2012] from SAO). Using a medium to large typical O4 SCD of 4 × 1043 molec2 cm−5 , we obtain an optical thickness of 3.6×10−3 at 344 nm [Thalman and Volkamer, 2013] and 6×10−4 at 328 nm [Lampel et al., 2018]. As both of these absorption peaks are larger than the BrO absorption shown in Figure 1, its impact should be discussed and analysed thoroughly in this manuscript and last but not least also included in Figure 1. These

absorption are well known and established (at least at 344 nm) as can be seen from the publications listed. As the bulk of the O4 absorption is found close to the surface, it's particularly sensitive to albedo changes and topography for satellite observation geometries. As mentioned by the other reviewers both factors play a role at the salt-lake and the Dead Sea Valley.

As part of the development of the OMBRO retrieval algorithm, a significant amount of effort was dedicated to algorithm "tuning", i.e., the optimization of elements in the retrieval process, including interfering absorbers like O_4. The spectral region of 343 nm, where O_4 has a small absorption feature, essentially is impossible to avoid in BrO retrievals: the fitting window would have to either terminate at shorter wavelengths or start past this feature, and both approaches yield to unacceptable low information content for the BrO retrievals to succeed. During the tuning process, we investigated the effects of, among many other things, including or excluding O_4, the use of different spectroscopic data sets (Greenblatt et al., 1990 and Hermans et al., 1999 cross-sections), shorter or longer wavelength windows for the retrieval, and even extending the retrieval window beyond the O_4 absorption feature but excluding the approximate wavelength slice of the feature itself. The only approach that provided quantitatively satisfactory results - i.e., stability of the retrieval under a wide range of conditions, minimized correlation with clouds, low fitting uncertainties, consistency of OMI global total column BrO with published results, and low noise in pixel-to-pixel retrievals - was to exclude O_4 from the fit. It is impossible to quantify O_4 atmospheric content from the absorption feature around 343 nm alone, and its correlation with absorption bands of BrO and CH_2O leads to spectral correlations in the course of the non-linear least squares minimization process that are detrimental to the OMI BrO retrievals. After the current OMBRO algorithm version was implemented Thalman (2013) cross-sections became available. The figure below shows the results of the fitting using different O_4 cross sections or not fitting O_4 for orbit 14035 (March 6 2007) over the Pacific Ocean The number of pixels with retrieved VCDs below 0 is 49 when O_4 is not fitted, 532 when using Hermans's cross-sections and 472 when using Thalman's cross-sections. The pixel to pixel noise, estimated as the standard deviation (only including pixels with cloud fractions below 30%) is always smaller when not fitting O_4. The estimation of the pixel to pixel noise is based in the assumption that over the Pacific Ocean longitudinal variability of BrO columns is small.

Table 1. Standard deviation of BrO VCDs [$x10^{13}$ mol. cm^{-2}] for different latitudinal bands for orbit 14035 (overflying the Pacific Ocean)

Latitudinal Band	No O_4	Hermans	Thalman
-90 to 90	**1.64**	**2.15**	**2.11**
60 to 90	**1.23**	**1.95**	**1.87**
30 to 60	**1.06**	**1.18**	**1.16**
0 to 30	**1.07**	**1.14**	**1.12**
-30 to 0	**0.97**	**1.03**	**1.02**
-60 to -30	**0.91**	**0.99**	**0.98**
-90 to -60	**0.89**	**1.61**	**1.49**

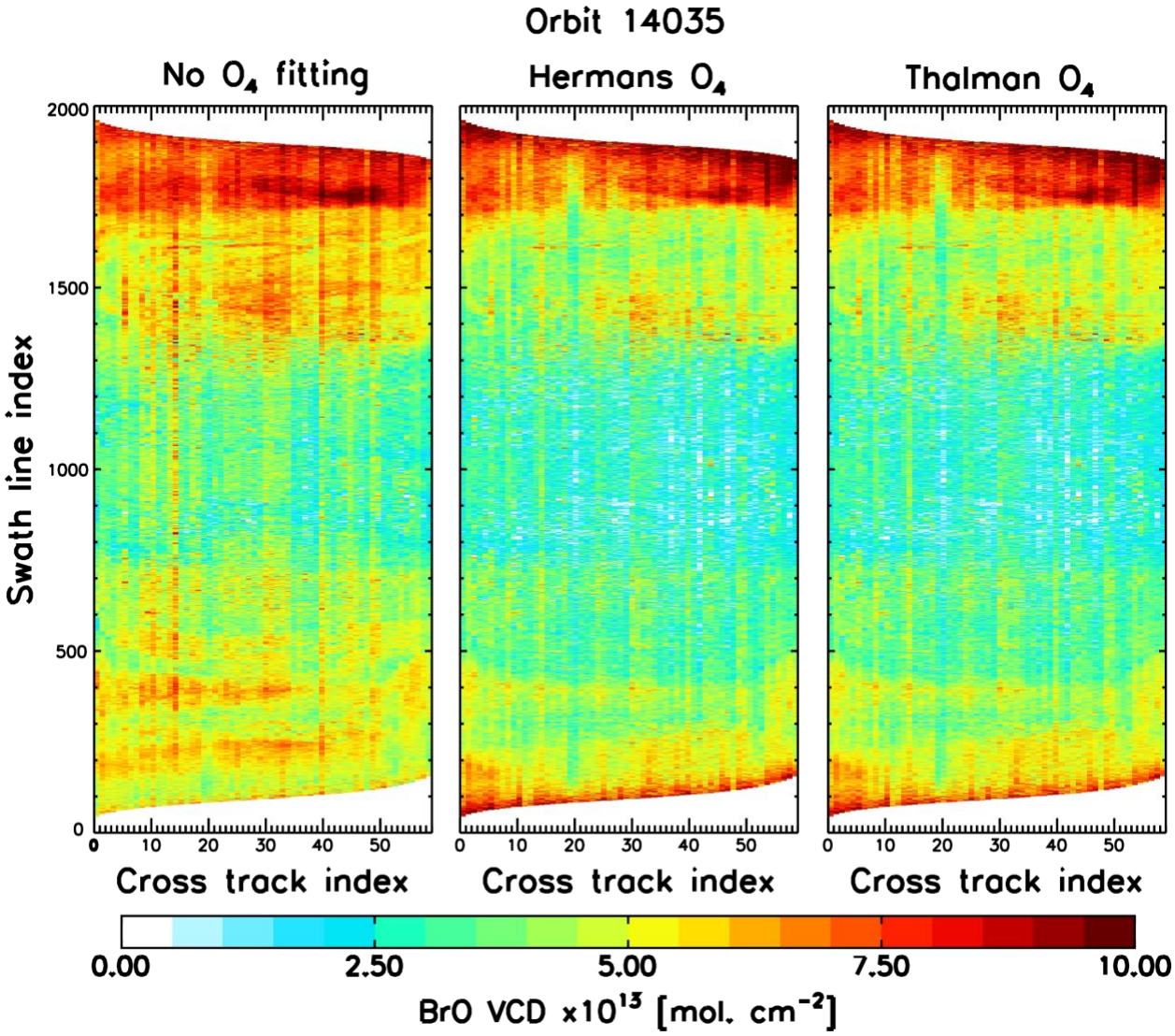

We have included the following text in the manuscript addressing our choice not to include O_4 cross sections:

As part of the development of the OMBRO retrieval algorithm, a significant amount of effort was dedicated to algorithm "tuning", i.e., the optimization of elements in the retrieval process, including interfering absorbers like O_4. The spectral region of 343 nm, where O_4 has a small absorption feature, essentially is impossible to avoid in BrO retrievals: the fitting window would have to either terminate at shorter wavelengths or start past this feature, and both approaches yield to unacceptable low information content for the BrO retrievals to succeed. During the tuning process, we investigated the effects of, among many other things, including or excluding O_4, the use of different spectroscopic data sets (Greenblatt et al., 1990 and Hermans et al., 1999 cross-sections), shorter or longer wavelength windows for the retrieval, and even extending the retrieval window beyond the O_4 absorption feature but excluding the approximate wavelength slice of the feature itself. The only approach that provided quantitatively satisfactory results - i.e., stability of the

retrieval under a wide range of conditions, minimized correlation with clouds, low fitting uncertainties, consistency of OMI global total column BrO with published results, and low noise in pixel-to-pixel retrievals- was to exclude O_4 from the fit. It is impossible to quantify O_4 atmospheric content from the absorption feature around 343 nm alone, and its correlation with absorption bands of BrO and CH_2O leads to spectral correlations in the course of the non-linear least squares minimization process that are detrimental to the OMI BrO retrievals.

This modified figure 1 shows in the bottom right panel the absorption due to the O_4 slant column suggested by the reviewer. We have included it here in the discussion to show its intensity, but given that based in the information provided above, we decide to exclude O_4 cross sections from the spectral fitting we think including it on the manuscript may lead to misunderstandings.

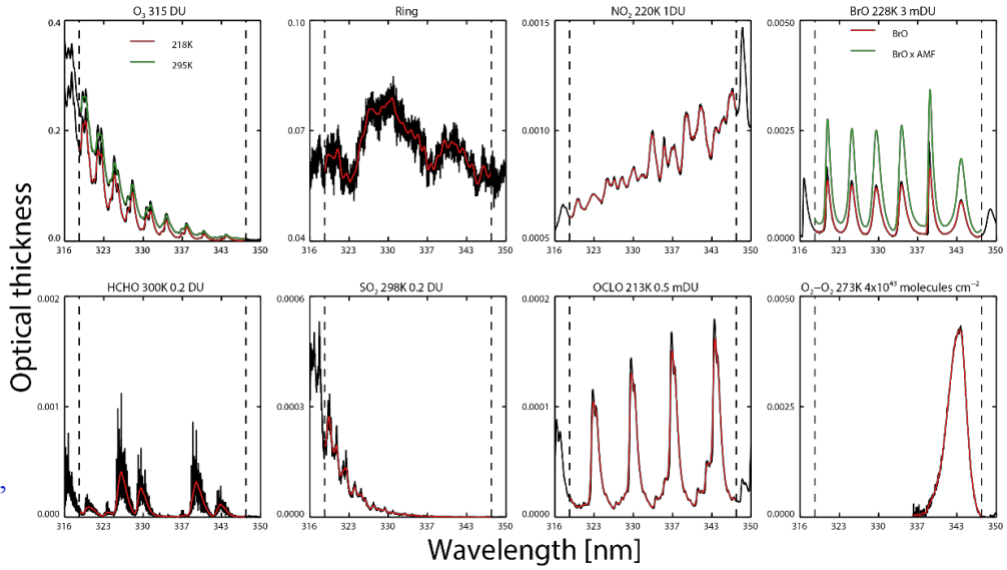

2. The AMFs for BrO are calculated and included in the fit, while the significantly stronger absorption of ozone is included without considering radiative transfer effects. Here an approach like the one presented in [Pukıte et al., 2010] could be applied, at least within the error analysis. These effects do not only appear in DOAS approaches, but also in intensity fitting or BOAS. [Vogel et al., 2013] showed that below 330 nm ozone absorption can have a large impact on the BrO results, at least if not considering these effects.

We study the impact of the approach described by Pukite et al., 2010 to correct the radiative transfer effects of the ozone absorption in our retrieval. The figure below shows the BrO VCDs obtained with the retrieval configuration we are describing in this paper for orbit OMI 14035 on the left panel. The middle panel shows the result for the same orbit after implementing the Pukite et al., method to correction ozone absorption radiative transfer effects and the right panel the difference expressed as the percentage. As suggested by the reviewer the differences are significant particularly at high SZA (latitudes). Between 60 degrees south and 60 degrees north the average difference is smaller than 10% with values around 2% near the equator. However, as we move near the poles with SZA above 60 degrees the differences start to be bigger reaching values of 30%.

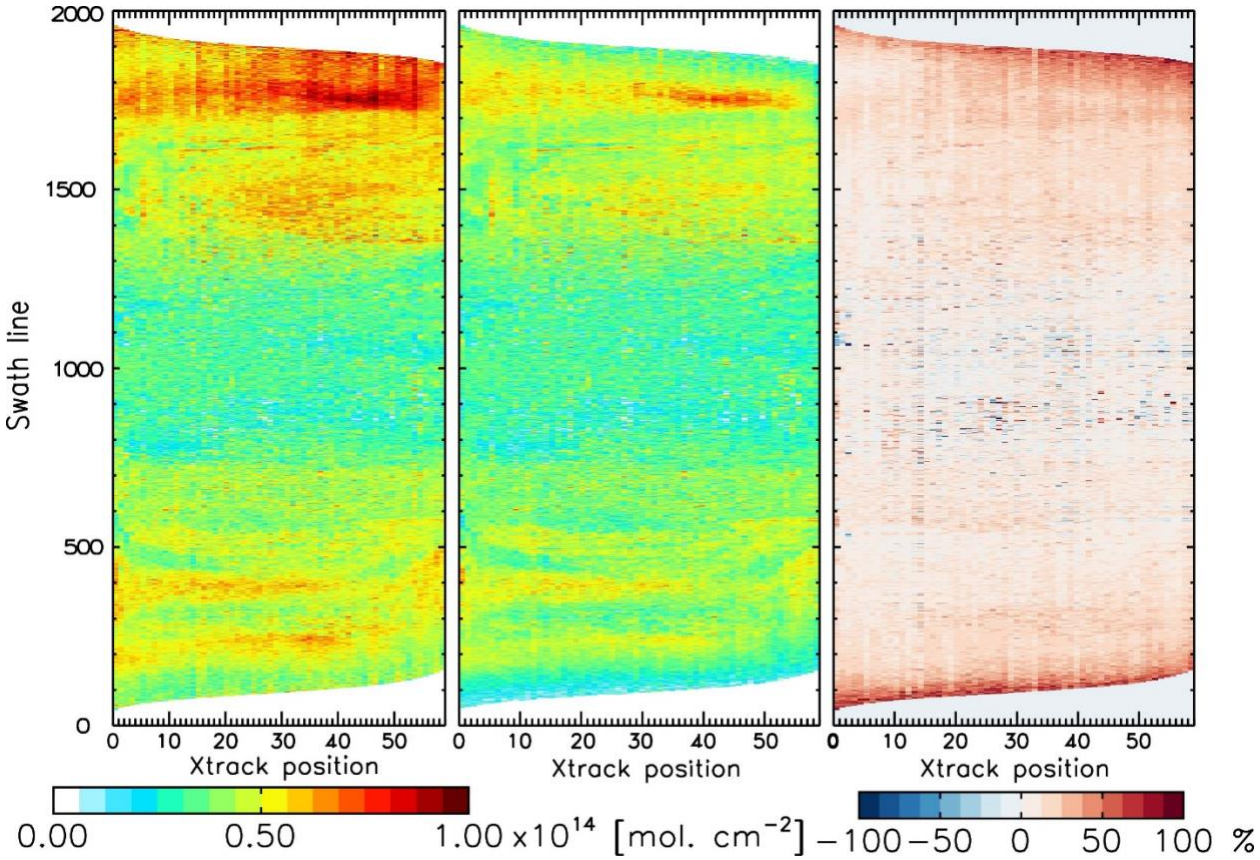

We have added the following sentences in section 3.5 to discuss this error source:

We study the impact of the approach described by Pukite et al., 2010 to correct the radiative transfer effects of the ozone absorption in our retrieval. We find that between 60 degrees south and 60 degrees north the average difference is smaller than 10% with values around 2% near the equator. However, as we move near the poles with SZA above 60 the differences are bigger arriving to mean values around 30% for SZA about 70 degrees.

3. A table of potential sources of interferences (literature cross-sections, fit settings, AMFs, uncertainties of other absorbers ..) and their magnitudes should be included in the manuscript. An example can be found at http://www.tropomi.eu/sites/default/files/files/S5P-BIRA-L2-ATBD-HCHO_400F_TROPOMI_v1p0p0-20160205.pdf and/or [De Smedt et al., 2012]. A list of current literature absorption cross-sections can also be found there. In general the observations on HCHO/BrO interferences from various DeSmedt et al publications are missing here and could also be of importance for BrO retrievals.

Section 3.5 has been renamed to "BrO VCD Error Analysis" has been updated with two additional tables.

We have investigated the sensitivity of OMI BrO VCD with respect to different retrieval windows. We have performed additional sensitivity studies, shown in Table 2, by excluding HCHO from the fitting, changing the reference spectra and changing the order of closure

polynomials. In these experiments, everything else is kept the same as in the operational retrieval. In Table 2, we list the median VCDs, median uncertainties and number of pixels with negative BrO for 13 July 2009 orbit number 26564.

Table 2. Error analysis studies.

Description	Median VCD (Molec. cm^{-2})	Median uncertainty (Molec. cm^{-2})	Number of negatives
Operational (V3)	3.89×10^{13}	7.85×10^{12}	1222
323.0 - 353.5 nm (V2)	2.69×10^{13}	1.01×10^{13}	4393
340.0 – 357.5 nm (V1)	2.48×10^{13}	1.29×10^{13}	9390
310.0 - 357.5 nm	1.91×10^{13}	6.83×10^{12}	7372
325.0 - 357.5 nm	3.10×10^{13}	8.75×10^{12}	3107
With O_2-O_2	3.57×10^{13}	8.65×10^{12}	1265
Online slit function	5.00×10^{13}	7.92×10^{12}	1003
Without common mode	3.72×10^{13}	1.11×10^{13}	2093
Without HCHO	2.53×10^{13}	6.93×10^{12}	1703

We followed your advice and perform similar analysis to Table. 9 in http://www.tropomi.eu/sites/default/files/files/S5P-BIRA-L2-ATBD-HCHO_400F_TROPOMI_v1p0p0-20160205.pdf.
A summary of the different error sources considered in the OMBRO vertical column error budget are presented in the Table below.

Error source	Type	Parameter uncertainty	Averaged uncertainty on BrO VCD	Evaluation method - reference
Measurement noise random	Random	S/N 500 - 1000	4-7x10^{12} molec. cm^{-2}	Error propagation;
HCHO	Systematic	Based on literature reported error estimates	5%	Chance and Orphal, 2011, 300K
O_3			2%	Malicet et al., 1995, 218K, 295K
BrO			8%	Wilmouth et al., 1999, 228K
NO_2			3%	Vandaele et al., 1998, 220K
SO_2			5%	Vandaele et al., 1994, 295K
OClO			5%	Kromminga et al., 2003, 213K
Ring			5%	Chance and Spurr, 1997
Offset order	Systematic	Vary polynomial order	10%	Sensitivity analysis

Polynomial order	Systematic	Vary polynomial order	10%	
Instrumental slit function and wavelength calibration	Systematic	Preflight and online slit function	28%	
Wavelength interval	Systematic	Varying fitting window	50%	

4. The spectral retrieval includes averaged residual spectra: The OMI ATBD V4 states: 'Remaining systematic residuals which are, by definition, uncorrelated to the trace gas spectra may be averaged and included in the spectrum fitting as a "common-mode" spectrum, to reduce the fitting rms and, proportionally, the fitting uncertainties, when they depend on the rms (eq. 5-3)'. This is not true as residuals are typically the result of an unaccounted absorber or effect and can be partially compensated for by the included absorptions, thus effectively resulting in erroneous SCDs. As typical residuals include contributions from various sources and due to various reasons, including them together as one spectrum links basically their relative sizes together and can therefore lead again to erroneous SCDs. The residual spectra can be used as a tool for data analysis (the missing O4 absorption should be easily visible if the residual spectra would have been inspected), but including the residual in the final fit lowers RMS, but not the measurement errors itself. It would be instructive to include a typical residual spectrum in the cross-section overview Figure 1.

We ran the retrieval with and without the common mode spectrum (residual spectra) for one orbit. The differences in VCD can be seen in this plot. While there is some dispersion there are mostly around a 1:1 line with very high correlation values. The plot includes in the legend the correlation values and the orthogonal regression of operational OMBRO (with common mode) and the retrieval without the common mode. Including the common mode

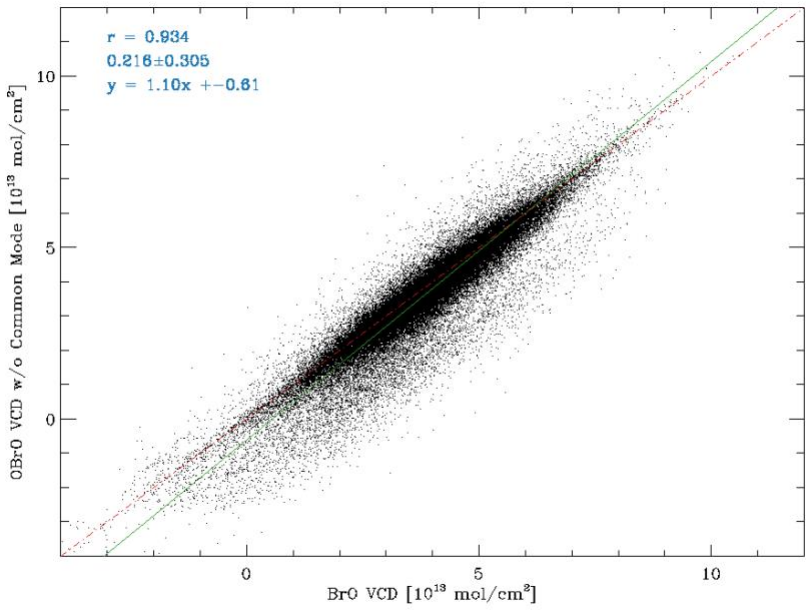

improves uncertainties as it can be seen in Table 2 (see answer to question number 3).

We have modified Figure 1 to include a mean residual illustrating a typical common mode spectrum (bottom right panel). We have also split different species with different optical depths in to different panels to address the suggestion made by the editor.

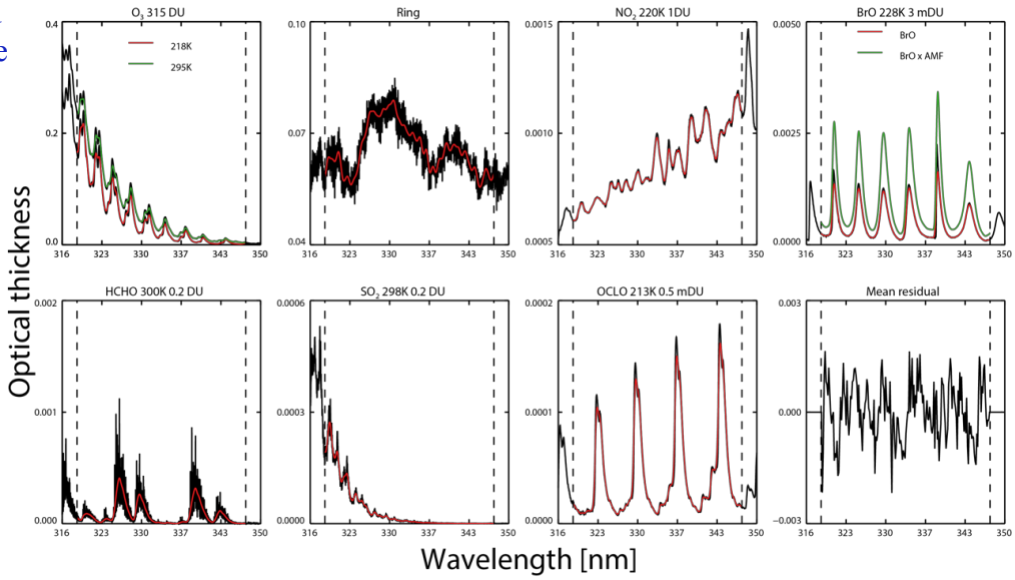

5. By mentioning tropospheric BrO from volcanoes and in polar regions it seems as if the data set can also be used for analysis of tropospheric BrO VCDs. However, as also stated in the manuscript, the AMF calculations assumed a stratospheric profile. Assuming typical tropospheric concentration profiles from the available literature error estimates could be provided. These cannot be found in the current revised manuscript. It is thus difficult if not impossible to use the OMBRO dataset for tropospheric applications. Depending on albedo, geometry and aerosol load could either under- or overestimate the real VCD. These errors need to be quantified for further reasonable use of this dataset by end-users.

As the reviewer indicated not considering tropospheric BrO can lead to errors up to 50% in function of the albedos and viewing geometry. The mean absolute difference between AMFs calculated using stratospheric only BrO profile and stratospheric-tropospheric profile is 41%. Section 3.5 Errors includes now the figure below and the following text describing the impact of the a-priori BrO profile in the AMF calculation:

To estimate the error associated with the AMFs calculations assuming a stratospheric profile we studied the difference between AMFs calculated using stratospheric only BrO profile and stratospheric-tropospheric profile and found that the mean absolute difference is 41%. Fig. 4 shows the AMF relative error dependency with wavelengths (bottom panel), albedo (middle panel) and VZA (top panel) as a function of the SZA. The AMFs relative errors are greater at high SZAs by about 50% for the case of wavelengths and VZAs.

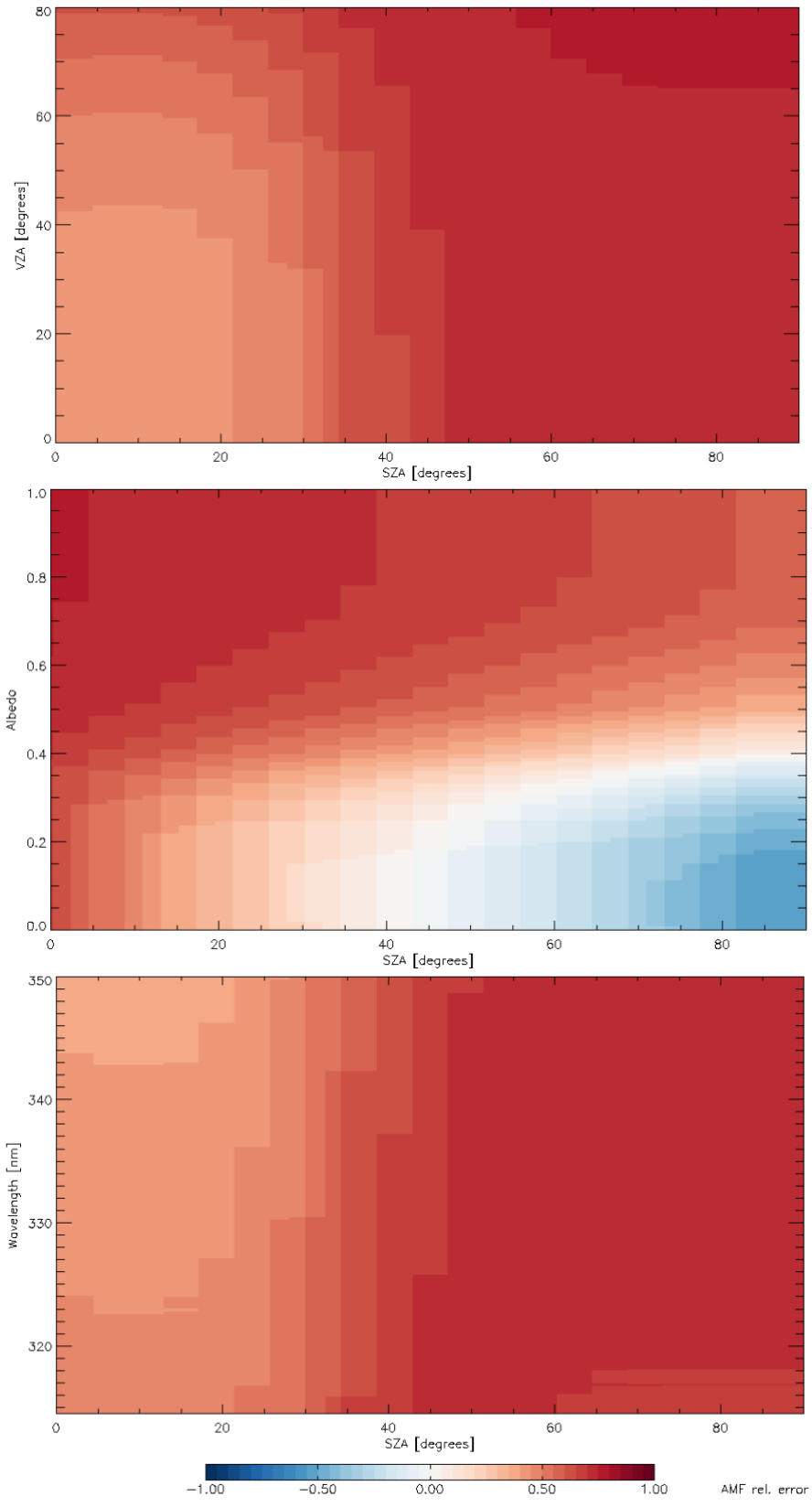
VZA [degrees]
SZA [degrees]
Albedo
SZA [degrees]
Wavelength [nm]
SZA [degrees]
−1.00
−0.50
0.00
0.50
1.00
AMF rel. error

Figure 4. AMFs relative errors as a function of SZA and wavelength (bottom panel), albedo (middle panel), and VZA (top panel).

6. p6-21: You use the preflight instrument function from Dirksen et al 2006. Is this for the BrO range consistent with the in-flight instrument function?
Sun et al., (2017) showed that the preflight slit functions for the UV2 channel of OMI shows very little cross-track variation (< 1% in FWHM), while the in-flight derived slit functions show a U-shaped cross-track dependency. This is particularly important at the edges of the swath. Sun et al., estimated the FWHM at large off-track viewing angles to be up to 5% broader than the nadir ones.

Is the instrument function of the respective OMI channels constant over time?
Kang et al., 2017 showed that the stability of the OMI slit function over time is remarkable. This can be seen in Figure 4 of Sun et al., 2017 which we have added as reference.

What is the impact of the findings presented by [Sun et al., 2017] on such a weak absorber as BrO?
Kang et al., assessed the impact of different slit functions by validating the retrieval results obtained with the different slit functions. This is a daunting task in the case of BrO not only because of the amount of reprocessing needed but also because of the limited availability of fiducial datasets for validation. Instead we can provide an estimation of the impact of the use of the pre-flight slit function and the on-flight slit function. Those results are commented in section 3.5. Table 2 contains the average values for orbit number 26564 for both cases.

The relevant text in section 3.5 is reproduced here:
We have analyzed the impact of using pre-flight measured or in-flight derived slit functions in the retrieval. The in-flight slit function has been simulated by a Gaussian function. The mean difference between retrievals using pre-flight and on-flight slit functions is error 14% (see Table 3). Table 2 contains the average values for orbit number 26564 for both cases.

For GOME-2 a north-south dependence was found due to temperature issues [Munro et al., 2015, Beirle et al., 2017]. This could be of importance for weak absorbers being overlayed by large absorptions and/or differences in instrument function between reference and measurement and could explain the need to include residual spectra in the fit (is that really needed?).
The OMI instrument has not been affected by this issue (Marchenko et al., 2015 and Schenkeveld et al., 2017).

Minor points:
1. mentioned also by other reviewers for the initial manuscript, again found in the revised manuscript: p6l12: comparison to DOAS fitting methods: Is this an advantage or disadvantage? What does this sentence add to the content of the manuscript? Looking at current DOAS evaluations (see e.g. [Wang et al., 2017]) you can see that high-pass filtering is often not applied, apart from the so called DOAS polynomial in OD-space, which is also used in the

presented manuscript. Please check again if all points of the initial reviews are considered in your revised manuscript.
We find the description in the text **"Unlike the often-used DOAS fitting method (Platt, 1994), radiances are not ratioed to irradiances, logarithms are not taken, and no high-pass filtering is applied."** to be an accurate description of the fitting method used in the algorithm presented here. Due to the extended use of the DOAS equation we find appropriate to highlight the differences with it.

2. The town Barrow is called Utqiagvik since 2016 (https://de.wikipedia.org/wiki/Utqiagvik). The name has been changed in the manuscript.

3. [Vogel et al., 2013] should be mentioned as the choice of the fit interval for BrO seems to be crucial for the reliability of the resulting data set. It contains a list of previously used fit settings which is missing within this manuscript.
We have included the following text in the manuscript.
For improved numerical stability, radiances and irradiances are divided by their respective averages over the fitting window, renormalizing them to values of ~1. BrO is fitted in the spectral window 319.0–347.5 nm, within the UV-2 channel of the OMI instrument. The switch from the previous fitting window of 340–357.5 nm to this shorter and wider fitting window is based on extensive sensitivity analysis following the method described by Vogel et al., 2013. This new fitting window aims at reducing the fitting uncertainty by including more BrO spectral structures as shown in Fig. 1 and reducing retrieval noise while preserving the stability of the algorithm. An analysis of the retrieval sensitivity to different windows is included in section 3.5.

4. How do the different OMBRO versions compare to each other? This could be also used to estimate the overall error margins.

We have included the following text in the manuscript comparing different OMBRO versions.

Table 2 shows the median VCD, median uncertainties and the number of negative pixels for the current operational version (V3), V2, and V1. Figure XX shows the monthly mean averages for V3.09 and V3.02 for the months of February and May of 2008. The differences on the VCD are about 30% in V3 comparing to V2. In comparison with V2 retrieval, the new retrieval (V9) does not show a large increase in the VCD concentrations, especially at the north polar region. The BrO background concentrations over the Pacific Ocean remain the same between the two versions, however, there are more retrieved VCDs.

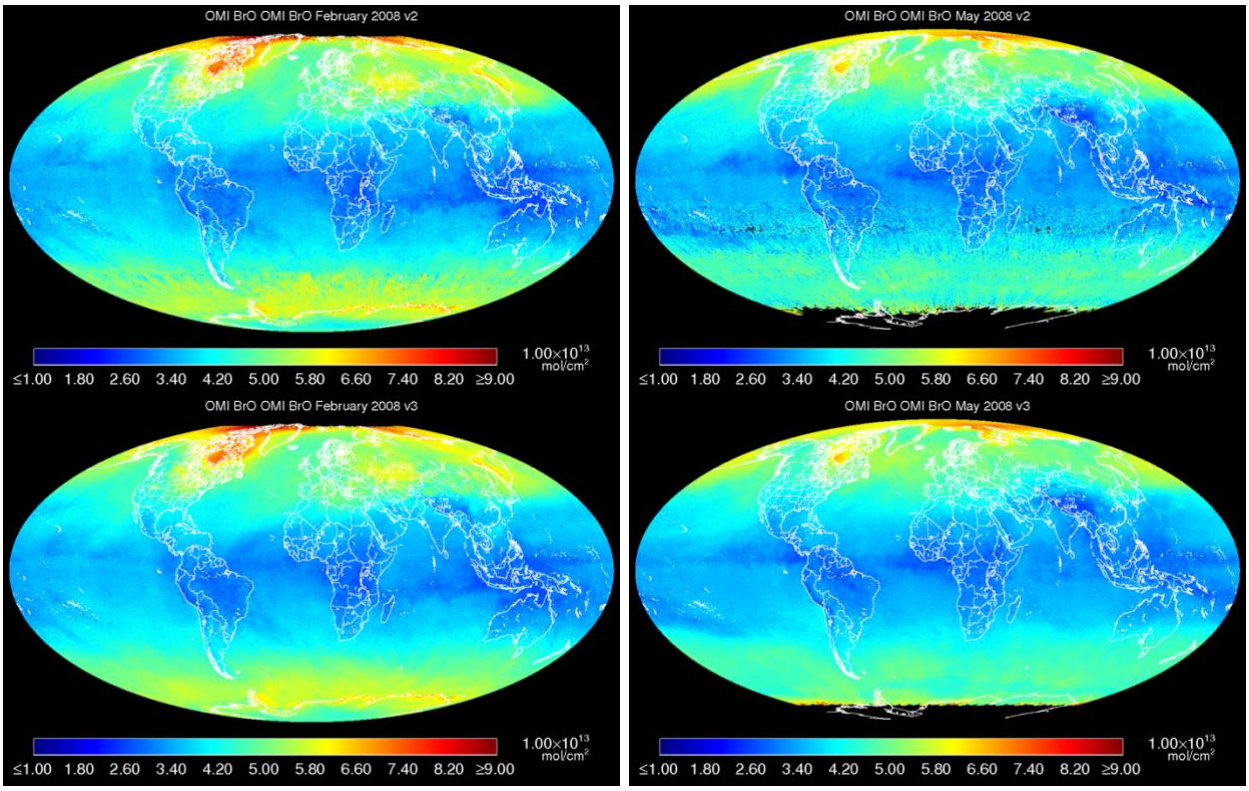

Figure 10. Monthly averages for February and May 2008 for version 3 and 2.

5. Please consider also more recent ozone literature cross-sections (e.g. [Serdyuchenko et al., 2014]) for future data products, as well as the temperature dependence of the Ring effect [Volkamer et al., 2015] and the Ring's wavelength dependence [Wagner et al., 2009] which is often compensated for in air-borne or groundbased analysis of scattered sun light spectra.
The references suggested above will be considered while developing future OMBRO retrievals.

6. The number of validation/comparison opportunities is especially low outside polar regions: How does the OMBRO data set compare quantitatively to the data presented in [Hörmann et al., 2016] for the Rann of Kutch?

We have done a preliminary analysis of salt water bodies including the Rann of Kutch. Although this work is not fully complete and will be a separate paper, however, we see maximum BrO VCDs appearing during March–May every year from 2004 – 2015 similar to what was reported by Hörmann et al., 2016. The BrO VCDs we see are around 4.5 x 10^{13} molecules cm^{-2}.

7. How do the VCDs from GOME2 compare quantitatively to those in OMBRO on a global scale and not only at nadir viewing direction? How do e.g. monthly means of both instruments compare to each other?

We have included the following text in the manuscript in section 4.1 comparing GOME2 and OMI. We also include the two figure below in our response.

In comparing the monthly averages of GOME2 data to OMBRO from February 2007 to December 2009 the seasonal variations are clearly seen. Our study show the mean VCDs for two different regions. GOME2 mean VCDs in the Pacific Ocean region are about 30% higher than those of OMI. However, in the polar region the mean VCDs are comparable for both instruments.

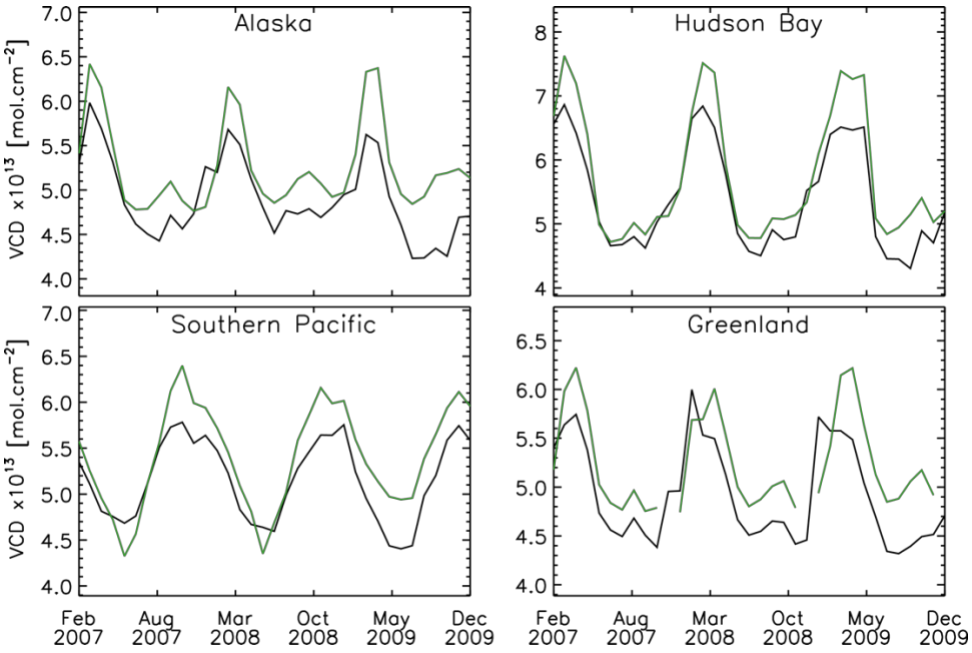

Figure 7. VCD of GOME2 (green) comparison to OMI (black) over four regions from February 2007 to December 2009 for four regions.

References

[De Smedt et al., 2012] De Smedt, I., Van Roozendael, M., Stavrakou, T., Müller, J.- F., Lerot, C., Theys, N., Valks, P., Hao, N., and van der A, R. (2012). Improved retrieval of global tropospheric formaldehyde columns from GOME-2/MetOp-A addressing noise reduction and instrumental degradation issues. Atmospheric Measurement Techniques, 5(11):2933–2949.

[Greenblatt et al., 1990] Greenblatt, G. D., Orlando, J. J., Burkholder, J. B., and Ravishankara, A. R. (1990). Absorption measurements of oxygen between 330 and 1140 nm. J. Geophys. Res., 95:18577–18582.

[Hermans et al., 1999] Hermans, C., Vandaele, A. C., Carleer, M., Fally, S., Colin, R., Jenouvrier, A., Coquart, B., and Mérienne, M.-F. (1999). Absorption cross-sections of atmospheric constituents: NO2, O2, and H2O. Environ. Sci. & Pollut. Res., 6(3):151–158.

[Hörmann et al., 2016] Hörmann, C., Sihler, H., Beirle, S., Penning de Vries, M., Platt, U., and Wagner, T. (2016). Seasonal variation of tropospheric bromine monoxide over the rann of kutch salt marsh seen from space. Atmospheric Chemistry and Physics, 16(20):13015–13034.

[Lampel et al., 2018] Lampel, J., Zielcke, J., Schmitt, S., Pöhler, D., Frieß, U., Platt, U., and Wagner, T. (2018). Detection of o4 absorption around 328 and 419nm in measured atmospheric absorption spectra. Atmospheric Chemistry and Physics, 18(3):1671–1683.

Marchenko, S., Krotkov, N. A., Lamsal, L. N., Celarier, E. A., Swartz, W. H., & Bucsela, E. J. (2015). Revising the slant column density retrieval of nitrogen dioxide observed by the Ozone Monitoring Instrument. Journal of Geophysical Research: Atmospheres, 120(11), 5670–5692. https://doi.org/10.1002/2014JD022913

[Pukıte et al., 2010] Puk,¯ıte, Janis, J., Kühl, S., Deutschmann, T., Platt, U., andWagner, T. (2010). Extending differential optical absorption spectroscopy for limb measurements in the UV. Atmospheric Measurement Techniques, 3(3):631–653.

[Richard et al., 2012] Richard, C., Gordon, I. E., Rothman, L. S., Abel, M., Frommhold, L., Gustafsson, M., Hartmann, J.-M., Hermans, C., Lafferty, W. J., Orton, G. S., et al. (2012). New section of the hitran database: Collision-induced absorption (cia). Journal of Quantitative Spectroscopy and Radiative Transfer, 113(11):1276–1285.

Schenkeveld, V. M. E., Jaross, G., Marchenko, S., Haffner, D., Kleipool, Q. L., Rozemeijer, N. C., … Levelt, P. F. (2017). In-flight performance of the Ozone Monitoring Instrument. Atmospheric Measurement Techniques, 10(5), 1957–1986. https://doi.org/10.5194/amt-10-1957-2017

[Serdyuchenko et al., 2014] Serdyuchenko, A., Gorshelev, V., Weber, M., Chehade, W., and Burrows, J. P. (2014). High spectral resolution ozone absorption crosssections - part 2: Temperature dependence. Atmospheric Measurement Techniques, 7(2):625–636.

[Sun et al., 2017] Sun, K., Liu, X., Huang, G., González Abad, G., Cai, Z., Chance, K., and Yang, K. (2017). Deriving the slit functions from omi solar observations and its implications for ozone-profile retrieval. Atmospheric Measurement Techniques, 10(10):3677–3695.

[Thalman and Volkamer, 2013] Thalman, R. and Volkamer, R. (2013). Temperature dependent absorption cross-sections of O2–O2 collision pairs between 340 and 630 nm and at atmospherically relevant pressure. Physical Chemistry Chemical Physics, 15(37):15371–15381.

[Vogel et al., 2013] Vogel, L., Sihler, H., Lampel, J., Wagner, T., and Platt, U. (2013). Retrieval interval mapping: a tool to visualize the impact of the spectral retrieval range on differential optical absorption spectroscopy evaluations. Atmospheric Measurement Techniques, 6(2):275–

299.

[Volkamer et al., 2015] Volkamer, R., Baidar, S., Campos, T. L., Coburn, S., DiGangi, J. P., Dix, B., Eloranta, E. W., Koenig, T. K., Morley, B., Ortega, I., Pierce, B. R., Reeves, M., Sinreich, R., Wang, S., Zondlo, M. A., and Romashkin, P. A. (2015). Aircraft measurements of bro, io, lyoxal, no2, h2o, o2-o2 and aerosol extinction profiles in the tropics: comparison with aircraft-/ship-based in situ and lidar measurements. Atmospheric Measurement Techniques, 8(5):2121–2148.

[Wagner et al., 2009] Wagner, T., Deutschmann, T., and Platt, U. (2009). Determination of aerosol properties from MAX-DOAS observations of the Ring effect. Atmospheric Measurement Techniques, 2(2):495–512.

[Wang et al., 2017] Wang, Y., Beirle, S., Hendrick, F., Hilboll, A., Jin, J., Kyuberis, A. A., Lampel, J., Li, A., Luo, Y., Lodi, L., Ma, J., Navarro, M., Ortega, I., Peters, E., Polyansky, O. L., Remmers, J., Richter, A., Rodriguez, O. P., Roozendael, M. V., Seyler, A., Tennyson, J., Volkamer, R., Xie, P., Zobov, N. F., and Wagner, T. (2017). Max-doas measurements of hono slant column densities during the madcat campaign: inter-comparison and sensitivity studies on spectral analysis settings. Atmospheric Measurement Techniques Discussions, 2017:1–38.

Changes in figures numbering

Old manuscript	Updated manuscript
Figure 1	Figure 1
Figure 2	Figure 2
Figure 3	Figure 3
----	Figure 4 is a new figure
Figure 4	Figure 5
Figure 5	Figure 6
----	Figure 7 is a new figure
Figure 6	Figure 8
Figure 7	Figure 9
---	Figure 10 is a new figure
Figure 8	Figure 11
Figure 9	Figure 12
Figure 10	Figure 13
Figure 11	Figure 14

OMI total bromine monoxide (OMBRO) data product: Algorithm, retrieval and measurement comparisons

Raid M. Suleiman[1], Kelly Chance[1], Xiong Liu[1], Gonzalo González Abad[1], Thomas P. Kurosu[2], Francois Hendrick[3], and Nicolas Theys[3]

[1]Harvard-Smithsonian Center for Astrophysics, Cambridge, MA, USA
[2]Jet Propulsion Laboratory, California Institute of Technology, Pasadena, CA, USA
[3]Royal Belgian Institute for Space Aeronomy, Brussels, Belgium

Correspondence to: Raid M. Suleiman (rsuleiman@cfa.harvard.edu)

Abstract. This paper presents the retrieval algorithm for the operational Ozone Monitoring Instrument (OMI) total bromine monoxide (BrO) data product (OMBRO) developed at the Smithsonian Astrophysical Observatory (SAO), and shows comparisons with correlative measurements and retrieval results. The algorithm is based on direct nonlinear least squares fitting of radiances from the spectral range 319.0-347.5 nm. Radiances are modeled from the solar irradiance, attenuated by contributions from BrO and interfering gases, and including rotational Raman scattering, additive and multiplicative closure polynomials, correction for Nyquist undersampling, and the average fitting residual spectrum. The retrieval uses albedo and wavelength-dependent air mass factors (AMFs), which have been pre-computed using a single mostly stratospheric BrO profile. The BrO cross sections are multiplied by the wavelength-dependent AMFs before fitting so that the vertical column densities (VCDs) are retrieved directly. The fitting uncertainties of BrO VCDs typically vary between 4 and 7×10^{12} molecules cm^{-2} (~10-20% of the measured BrO VCDs). The retrievals agree well with GOME-2 observations at simultaneous nadir overpasses and ground-based zenith-sky measurements at Harestua, Norway, with mean biases less than $-0.216\pm1.13\times10^{13}$ molecules cm^{-2} and $0.12\pm0.76\times10^{13}$ molecules cm^{-2}, respectively. Global distribution and seasonal variation of OMI BrO are generally consistent with previous satellite observations. Global distribution of BrO from OMBRO shows spatial and temporal patterns similar to GOME-2 retrievals. The OMBRO retrievals show enhancement of BrO over U.S. Great Salt Lake. It also shows significant BrO enhancement from the eruption of the Eyjafjallajökull volcano, although the BrO retrievals are affected under high SO_2 loading conditions by the sub-optimum choice of SO_2 cross sections.

1 Introduction

Bromine monoxide (BrO) is a halogen oxide, predominantly located in the stratosphere and upper troposphere where, like chlorine monoxide (ClO), it is a catalytic element in the destruction of stratospheric ozone (von Glasow *et al*., 2004; Salawitch *et al*., 2005), but with higher efficiency per molecule. Sources of tropospheric BrO include bromine release ("explosions") during the Polar Spring (Hausmann and Platt, 1994; Hollwedel *et al*., 2004; Simpson *et al.*, 2007; Begoin *et al*., 2010; Salawitch *et al*., 2010; Abbatt, *et al*., 2012; Blechschmidt *et al*., 2016), volcanic eruptions (Bobrowski *et al.*, 2003; Chance, 2006; Theys *et al.*, 2009;), salt lakes (Hebestreit, *et al.*, 1999; Hörmann *et al*. 2016) and stratospheric transport (Salawitch *et al*., 2010). Global BrO measurements from space were first proposed for the Scanning Imaging Absorption Spectrometer for Atmospheric Cartography (SCIAMACHY) instrument (Chance *et al*., 1991) and were first demonstrated with Global Ozone Monitoring Experiment (GOME-1) measurements (Chance, 1998; Platt and Wagner, 1998; Richter *et al*., 1998), and since with SCIAMACHY nadir (Kühl *et al*., 2008) and Global Ozone Monitoring Experiment 2 (GOME-2) measurements (Theys *et al*., 2011; Toyota *et al*., 2011). Initial observations of BrO by OMI were first reported by Kurosu *et. al*. (2004). Polar Spring BrO enhancements are known to be associated with boundary layer ozone depletion (Hausmann and Platt, 1994; von Glasow *et al*., 2004; Salawitch *et al*., 2005; Simpson *et al.*, 2007; Salawitch *et al*., 2010; Abbatt, *et al*., 2012). OMI measurements of BrO have been used together with chemical and dynamical modeling to investigate stratospheric versus tropospheric enhancements of atmospheric BrO at high northern latitudes (Salawitch *et al*., 2010). OMI BrO retrieval using the Differential Optical Absorption Spectroscopy (DOAS) method has been used to study the seasonal variations of tropospheric bromine monoxide over the Rann of Kutch salt marsh (Hörmann *et al*. 2016). The Arctic Research of the Composition of the Troposphere from Aircraft and Satellites (ARCTAS) campaign (Choi *et al*., 2012) found consistency between BrO column densities calculated from Chemical Ionization Mass Spectrometer (CIMS) measurements with the tropospheric BrO columns derived from OMI using our operational retrieval algorithm. BrO has been observed from the ground in Harestua, Norway (Hendrick *et al*., 2007), Lauder, New Zealand (Schofield *et al*., 2004a, 2004b), Antarctica (Schofield *et al*., 2006), Utqiagvik (Barrow), Alaska (Liao et al., 2011; Frieß et al., 2011; Liao et al., 2012; Sihler *et al.*, 2012; Peterson *et al.*, 2016), Eureka, Canada (Zhao *et al.*, 2015), Summit, Greenland (Stutz *et al.*, 2011) and the Arctic Ocean (Burd *et al.*, 2017).

Formatted: Font:Not Bold, Complex Script Font: Bold

Moved down [1]: ; Simpson *et al.*, 2007; Abbatt, *et al*., 2012

Moved (insertion) [1]

Deleted: Bromine monoxide (BrO) is a halogen oxide, predominantly located in the stratosphere and upper troposphere where, like chlorine monoxide (ClO), it is a catalytic element in the destruction of stratospheric ozone (Hausmann and Platt, 1994); von Glasow *et al*., 2004; Salawitch *et al*., 2005; Simpson *et al.*, 2007; Abbatt, *et al*., 2012), but with higher efficiency per molecule. Sources of tropospheric BrO include bromine release ("explosions") during the Polar Spring (Hollwedel *et al*., 2004; Begoin *et al*., 2010; Salawitch *et al*., 2010; ; Simpson *et al.*, 2007; Abbatt, *et al*., 2012Blechschmidt *et al*., 2016), volcanic eruption (Bobrowski *et al*., 2003; Chance, 2006; Theys *et al*., 2009;), salt lakes (Hebestreit, *et al*., 1999; Hörmann *et al*. 2016) and stratospheric transport (Salawitch *et al*., 2010). Global BrO measurements from space were first proposed for the Scanning Imaging Absorption Spectrometer for Atmospheric Cartography (SCIAMACHY) instrument (Chance *et al*., 1991) and were first demonstrated with Global Ozone Monitoring Experiment (GOME-1) measurements (Chance, 1998; Platt and Wagner, 1998; Richter *et al*., 1998), and since with SCIAMACHY nadir (Kühl *et al*., 2008) and Global Ozone Monitoring Experiment 2 (GOME-2) measurements (Theys *et al*., 2011).

Deleted: and

Deleted: a,b

Deleted: Canada (

Formatted: Font:Bold, Font color: Accent 1, English (UK)

Enhancement of BrO in the vicinity of salt lakes like the Dead Sea and the Great Salt Lake have been observed from ground-based measurements (Hebestreit *et al.*, 1999; Matveev *et al.,* 2001; Stutz *et al.*, 2002; Tas et al., 2005; Holla *et al.,* 2015). The active bromine compound release is due to the reaction between atmospheric oxidants with salt reservoirs. Satellite observation of salt lake BrO was first reported over the Great Salt Lake and the Dead Sea from OMI (Chance, 2006; Hörmann *et al*. 2016). Seasonal variations of tropospheric BrO over the Rann of Kutch salt marsh have been observed using OMI from an independent research BrO product (Hörmann *et al*. 2016). Bobrowski *et al*. (2003) made the first ground-based observations of BrO and SO_2 abundances in the plume of the Soufrière Hills volcano (Montserrat) by multi-axis DOAS (MAX-DOAS). BrO and SO_2 abundances as functions of the distance from the source were measured by MAX-DOAS in the volcanic plumes of Mt. Etna in Sicily, Italy and Villarica in Chile (Bobrowski *et al*., 2007). The BrO/SO_2 ratio in the plume of Nyiragongo and Etna was also studied (Bobrowski *et al*., 2015). The first volcanic BrO measured from space was from the Ambrym volcano, measured by OMI (Chance, 2006). Theys *et al*. (2009) reported on GOME-2 detection of volcanic BrO emission after the Kasatochi eruption. Hörmann *et al.* (2013) examined GOME-2 observations of BrO slant column densities (SCDs) in the vicinity of volcanic plumes; it showed clear enhancements of BrO in ~1/4 of the volcanos, and revealed large spatial differences in BrO/SO_2 ratios.

Formatted: Subscript

The purpose of this paper is to describe the OMI BrO operational algorithm and the data product, compare it with ground-based and other satellite measurements and analyze its spatiotemporal characteristics. This paper is organized as follows: Section 2 describes the OMI instrument and the data product. Section 3 gives a detailed description of the operational algorithm including algorithm and product history, spectral fitting, AMF calculations, destriping, and fitting uncertainties. Section 4 presents results and discussion including comparison with GOME-2 and ground-based zenith-sky measurements at Harestua, Norway, global distribution, seasonality, enhanced BrO from the U.S. Great Salt Lake and Iceland's Eyjafjallajökull volcano. Section 5 concludes this study.

2 OMI instrument and OMBRO data product

2.1 OMI instrument

OMI was launched on the NASA Earth Observing System (EOS) Aura satellite into a sun-synchronous orbit on 15 July 2004. It is a push-broom imaging spectrometer that observes solar backscattered radiation in the visible and ultraviolet from 270-500 nm in three channels (UV1: 270-310 nm, UV2: 310-365 nm, visible: 350-500 nm) at spectral resolution of 0.42-0.63 nm and spatial resolution in the normal (global sampling) mode ranging from 13×24 km^2 at direct nadir to about 28×150 km^2 at the swath edges. The global mode (GM) has 60 ground pixels with a total cross-track swath of 2600 km. There are also spatial and spectral zoom modes with twice finer across-track spatial resolution at nadir. The spatial zoom mode (SZM) is employed every 32 days (Levelt *et al*., 2006): data from this mode are spatially rebinned to global-mode sampling sizes, known as the rebinned spatial zoom mode. The SZM, like the global mode (GM), has 60 cross-track pixels. These are re-binned to 30 pixels, to form "the rebinned spatial zoom mode" (RSZM) which is equivalent in pixel size to the GM data, but with reduced spatial coverage.

Since June 2007, certain cross-track positions of OMI data have been affected by the row anomaly (http://projects.knmi.nl/omi/research/product/rowanomaly-background.php): some loose thermal insulating material likely appeared in front of the instrument's entrance slit, which can block and scatter the light thus causing errors in level 1b data and subsequently the level 2 retrievals (Kroon *et al.*, 2011). Initially, the row anomaly only affected a few positions and the effect was small. But since January 2009, the anomaly has become more serious, spreading to ~1/3 of the positions and retrievals at those positions are not recommended for scientific use. A flagging field has been introduced in the OMI level 1b data to indicate whether an OMI pixel is affected by this instrument anomaly.

OMI measures ozone and other trace gases, aerosols, clouds, and surface properties. Products developed at the SAO include operational BrO, chlorine dioxide (OClO), and formaldehyde (H_2CO; González Abad *et al*., 2015) that are archived at NASA Goddard Earth Sciences (GES) Data and Information Services Center (DISC), and offline ("pre-operational") ozone profile and tropospheric ozone (O_3) (Liu *et al*., 2010; Huang *et al.*, 2017, 2018), glyoxal ($C_2H_2O_2$) (Chan Miller *et al*., 2014, 2016) and water vapor (H_2O) (Wang *et al*., 2014, 2016) that are available at

the Aura validation data center (AVDC). All the products except for the ozone profile product are produced using nonlinear least-squares (NLLS) fitting methods based on those previously developed at the SAO for the analysis of measurements from the GOME (now GOME-1) (Chance, 1998; Chance, *et al*., 2000) and SCIAMACHY instruments (Burrows and Chance, 1991; Chance *et al*., 1991; Martin *et al.*, 2006).

2.2 OMBRO data product

The current operational BrO product, OMBRO version 3, contains BrO vertical column densities (VCDs), slant column densities (SCDs), effective air mass factors (AMFs) and ancillary information retrieved from calibrated radiance and irradiance spectra in OMI GM and RSZM level 1b data product. Each BrO product file contains a single orbit of data, from pole to pole, for the sunlit portion of the orbit. The data product from 26 August 2004 through the present is available at GES DISC. Data used in this study cover the period from 1 January 2005 to 31 December 2014.

Deleted: .0.5

3 Retrieval algorithm

3.1 Algorithm and product history

OMBRO Version 1.0 was released on 1 February 2007, based on a spectral fitting window of 338–357 nm. Version 2.0 was released on 13 April 2008. It included major adjustments for Collection 3 Level 1b data, improved destriping measures, change of the fitting window to 340–357.5 nm, improvements to radiance wavelength calibration, and several improvements for processing near-real-time data. In both Versions 1 and 2, total BrO VCDs were retrieved in two steps: first performing spectral fitting using the basic optical absorption spectroscopy (BOAS) method to derive SCDs from OMI radiance spectra, and then converting from SCDs to VCDs by dividing AMFs. This is similar to current SAO H_2CO, H_2O and $C_2H_2O_2$ as mentioned previously. The latest Version 3.0.5, released on 28 April 2011, includes major algorithm changes: the fitting window was moved to 319.0–347.5 nm, and BrO cross sections are multiplied by wavelength-dependent AMFs, which are a function of albedo, before fitting, for a direct retrieval of BrO VCDs. SCDs are similarly retrieved in a separate step by fitting BrO cross sections that have not been multiplied with wavelength-dependent AMFs, and an effective AMF = SCD/VCD is computed. Diagnostic

cloud information from the OMCLDO2 product (Acarreta *et al.*, 2004) was added, and the row-anomaly indicating flags were carried over from the level 1b product.

The current algorithm is described in detail in the rest of this section, with spectral fitting in Section 3.2, AMF calculation prior to spectral fitting in Section 3.3, post-processing de-stripping to remove cross-track dependent biases in Section 3.4, and fitting uncertainties and error estimates in Section 3.5.

3.2 Spectral fitting

Most aspects of the algorithm physics for the direct fitting of radiances by the BOAS method were developed previously at SAO for analysis of GOME and SCIAMACHY satellite spectra (Chance, 1998, Chance *et al*., 2000, OMI, 2002; Martin *et al.*, 2006) and in the various algorithm descriptions of other SAO OMI products (Wang *et al*., 2014; Chan Miller *et al*., 2014; Gonzalez Abad *et al*., 2015). Unlike the often-used DOAS fitting method (Platt, 1994), radiances are not ratioed to irradiances, logarithms are not taken, and no high-pass filtering is applied.

The spectral fitting in the SAO OMI BrO retrieval is based on a Gauss-Newton NLLS fitting procedure, the CERN ELSUNC procedure (Lindström and Wedin, 1987), which provides for bounded NLLS fitting. Processing begins with wavelength calibration for both irradiance and radiance. In each case the wavelength registration for the selected fitting window is determined independently for each cross-track position by cross-correlation of OMI spectra with a high spectral resolution solar irradiance (Caspar and Chance, 1997; Chance, 1998; Chance and Kurucz, 2010) using the preflight instrument slit functions (Dirksen *et al*., 2006). To improve cross-track stripe correction (Section 3.4) and reduce the noise in the solar irradiance data, the OMI irradiance spectra are composites derived from a principal component analysis of three years of individual OMI irradiance measurements (2005-2007). Radiance wavelength calibration is performed for a representative scan line of radiance measurements (usually in the middle of the orbit) to determine a common wavelength grid for reference spectra.

Following wavelength correction, an undersampling correction spectrum is computed to partially correct for spectral undersampling (lack of Nyquist sampling: Chance, 1998; Slijkhuis *et al*., 1999;

Chance *et al*., 2005). The calculation of the corrections for the undersampling is accomplished by convolving the preflight slit functions with the high-resolution solar spectrum and differencing its fully-sampled and undersampled representations (Chance *et al*., 2005).

Fitting is then performed for all scan lines in the OMI swath granule. In each stage, the fitting is performed individually for the 60 cross-track pixels of a block of 100 OMI across-track swath lines along the flight direction (30 cross-track pixels for the RSZM) according to Eq. (1):

$$I = \{(aI_0 + \sum_i \alpha_i A_i) e^{-\sum_j \beta_j B_j} + \sum_k \gamma_k C_k\} Poly_{scale} + Poly_{baseline}\,, \quad (1)$$

where I_0 is the solar irradiance (used in our operational BrO retrieval) or radiance reference measurement, I is the Earthshine radiance (detected at satellite), a is albedo, α_i, β_j, γ_k, are the coefficients to the reference spectra of A_i, B_j, C_k, (for example, trace gas cross sections, Ring effect, vibrational Raman, undersampling correction, common mode, *etc*.) of model constituents. The reference spectra are derived separately for each cross-track position from original high-resolution cross sections convolved with the corresponding OMI slit functions after correcting for the solar I_0 effect (Aliwell *et al.*, 2002). Fig. 1 shows the trace gas cross sections and Ring spectra used in the current operational algorithm. The black lines are the original high-resolution reference spectra, and the color lines show the corresponding spectra convolved with OMI slit function, which are used in the fitting.

For improved numerical stability, radiances and irradiances are divided by their respective averages over the fitting window, renormalizing them to values of ~1. BrO is fitted in the spectral window 319.0–347.5 nm, within the UV-2 channel of the OMI instrument. The switch from the previous fitting window of 340–357.5 nm to this shorter and wider fitting window is based on extensive sensitivity analysis following the method described by Vogel et al., 2013. This new fitting window aims at reducing the fitting uncertainty by including more BrO spectral structures as shown in Fig. 1 and reducing retrieval noise while preserving the stability of the algorithm. An analysis of the retrieval sensitivity to different windows is included in section 3.5.

Deleted: For improved numerical stability, radiances and irradiances are divided by their respective averages over the fitting window, renormalizing them to values of ~1. BrO is fitted in the spectral window 319.0–347.5 nm, within the UV-2 channel of the OMI instrument. The switch from the previous fitting window of 340–357.5 nm to this shorter and wider fitting window is to reduce fitting uncertainty by including more BrO spectral structures as shown in Fig. 1.

Formatted: Complex Script Font: Bold

The rotational Raman scattering (Chance and Spurr, 1997; Chance and Kurucz, 2010) and undersampling correction spectra, A_i, are first added to the albedo-adjusted solar irradiance aI_0, with coefficients α_i as shown in Eq. 1. Radiances I are then modeled as the this quantity attenuated by absorption from BrO, O_3, NO_2, H_2CO, and SO_2 with coefficients β_j fitted to the reference spectra B_j as shown in Eq. 1. A common mode spectrum C_k, computed on line, is added by fitting coefficient γ_k after the Beer-Lambert law contribution terms. An initial fit of several hundred pixels per cross-track position determines the common mode spectra (one spectrum per cross-track position, between 30°N and 30°S) as the average of the fitting residuals. The common mode spectra include any instrument effects that are uncorrelated to molecular scattering and absorption. This is done to reduce the fitting root-mean-square (RMS) residuals, and the overall uncertainties. These are then applied as reference spectra in fitting of the entire orbit. The fitting additionally contains additive ($Poly_{baseline}$) and multiplicative closure polynomials ($Poly_{scale}$), parameters for spectral shift and, potentially, squeeze (not normally used). The operational parameters and the cross sections used are provided in Table 1.

As part of the development of the OMBRO retrieval algorithm, a significant amount of effort was dedicated to algorithm "tuning", i.e., the optimization of elements in the retrieval process, including interfering absorbers like O_4. The spectral region of 343 nm, where O_4 has a small absorption feature, essentially is impossible to avoid in BrO retrievals: the fitting window would have to either terminate at shorter wavelengths or start past this feature, and both approaches yield to unacceptable low information content for the BrO retrievals to succeed. During the tuning process, we investigated the effects of, among many other things, including or excluding O_4, the use of different spectroscopic data sets (Greenblatt et al., 1990 and Hermans et al., 1999 cross-sections), shorter or longer wavelength windows for the retrieval, and even extending the retrieval window beyond the O_4 absorption feature but excluding the approximate wavelength slice of the feature itself. The only approach that provided quantitatively satisfactory results - i.e., stability of the retrieval under a wide range of conditions, minimized correlation with clouds, low fitting uncertainties, consistency of OMI global total column BrO with published results, and low noise in pixel-to-pixel retrievals - was to exclude $O_4$from the fit. It is impossible to quantify O_4 atmospheric content from the absorption feature around 343 nm alone, and its correlation with

Formatted: Font:Not Bold, Complex Script Font: Bold

Formatted: Font:Not Bold, Complex Script Font: Bold

Formatted: Font:Not Bold, Complex Script Font: Bold

absorption bands of BrO and CH_2O leads to spectral correlations in the course of the non-linear least squares minimization process that are detrimental to the OMI BrO retrievals.

Formatted: English (UK)

3.3 Air mass factors

Due to significant variation in ozone absorption and Rayleigh scattering in the fitting window AMFs vary with wavelength by 10-15% as shown in Fig. 2. At large solar and viewing zenith angles it is difficult to identify a single representative AMF *ad hoc*. The wavelength dependent AMFs are introduced to take into account for such strong variation within the BrO fitting window. They are applied pre-fit to the BrO cross sections, and the spectral fit retrieves VCDs directly. This direct fitting approach is a major departure from the commonly employed 2-step fitting procedure (OMI, 2002). It was first developed for retrievals of trace gases from SCIMACHY radiances in the shortwave infrared (Buchwitz *et al*., 2000) and has been demonstrated for total O_3 and SO_2 retrievals from GOME/SCIAMACHY measurements in the ultraviolet (Bracher *et al.*, 2005; Coldewey-Egbers *et al*., 2005; Weber et al., 2005; Lee *et al.,* 2008).

The albedo- and wavelength-dependent AMFs were pre-computed with the Linearized Discrete Ordinate Radiative Transfer code (LIDORT, Spurr, 2006) using a single mostly stratospheric BrO profile (Fig. 3, left panel). The BrO profile, based on the model of Yung *et al.* (1980), has ~30% BrO below 15 km, ~10% BrO below 10 km, and ~2% BrO below 5 km. For conditions with enhanced BrO in the lower troposphere, using this profile will overestimate the AMFs and therefore underestimate the BrO VCDs. The AMF profile used can lead to errors up to 50% with variations of albedos and viewing geometry. The mean absolute difference between AMF calculations using the stratospheric profile and the stratospheric-tropospheric profile (Fig. 3, right panel) is 41%. Surface albedos are based on a geographically varying monthly mean climatology derived from OMI (Kleipool *et al.,* 2008). Although AMFs based on this BrO profile only slightly depend on surface albedo, albedo effects can be significant over highly reflective snow/ice surfaces, reducing VCDs by 5-10%.

In order to provide the AMF in the data product for consistency with previous versions based on a two-step approach, a second fitting of all OMI spectra is performed with unmodified BrO cross sections, which yields SCDs. An effective AMF can then be computed as AMF = SCD/VCD.

The green line in the top right panel of Fig. 1 shows the modified BrO cross section after multiplication with the wavelength-dependent AMF (albedo = 0.05, SZA (Solar Zenith Angle) = 5.0°, and VZA (Viewing Zenith Angle) = 2.5°). The wavelength-dependence in AMF is visible from the varying differences near BrO absorption peaks and the right wings at different wavelengths. The correlation of the unmodified BrO cross sections with the rest of the fitted molecules is small (typically less than 0.12), except with H_2CO (0.43). However, it is safe to assume that in most polar regions with enhanced BrO there are no high concentrations of formaldehyde. It will be worthwhile for future studies to assess the interference of H_2CO under high H_2CO and background BrO conditions similar to De Smedt et al., 2015. In addition, the AMF wavelength dependence increases with the increase of solar and viewing zenith angles and surface albedo, which increases the correlation between modified BrO cross sections and O_3 cross sections. However, the correlation with O_3 becomes noticeable (~0.10) only at SZAs above ~80°.

Deleted: salmon color line in bottom

Deleted: =

Deleted: =

Deleted: solar zenith angles

3.4 Destriping

OMI L1b data exhibit small differences with cross-track position, due to differences in the dead/bad pixel masks (cross-track positions are mapped to physically separate areas on the CCD), dark current correction, and radiometric calibration, which lead to cross-track stripes in Level 2 product (Veihelmann and Kleipool, 2006). Our destriping algorithm employs several methods to reduce cross-track striping of the BrO columns. First, we screen outliers in the fitting residuals. This method, originally developed to mitigate the effect of the South Atlantic Anomaly in SAO OMI BrO, H_2CO, and OClO data products, is now also being employed for GOME-2 (Richter *et al.*, 2011). Screening outliers is done through computing the median, r_{med}, and the standard deviation σ of residual spectra $r(\lambda)$ and in subsequent refitting excluding any spectral points for which $r(\lambda) \geq |r_{med} \pm 3\sigma|$. This can be done repeatedly for every ground pixel, which makes the processing slow. However, we do it once for a reference scan line, recording the positions of the bad pixels, and excluding them by default in each subsequent fit. Second, after the completion of

the spectral fitting process for all ground pixels in the granule, a post-processing cross-track bias correction is performed: an average cross-track pattern is calculated from the along-track averages of all BrO VCDs for each cross-track position within a ±30° latitude band around the equator, to which a low-order polynomial is fitted. The differences between the cross-track pattern and the fitted polynomial is then applied as a cross-track VCD correction (or "smoothing") factor. The smoothed VCDs are provided in a separate data field, *ColumnAmountDestriped*. Smoothed SCDs are derived in an analogous fashion and are also included in the data product.

3.5 BrO VCD Error Analysis

Deleted: Fitting uncertainties

Estimated fitting uncertainties are given as $\sigma_i = \sqrt{C_{ii}}$ where C is the covariance matrix of the standard errors. This definition is strictly true only when the errors are normally distributed. In the case where the level 1 data product uncertainties are not reliable estimates of the actual uncertainties, spectral data are given unity weight over the fitting window, and the 1σ fitting error in parameter i is determined as

$$\sigma_i = \varepsilon_{rms}\sqrt{\frac{c_{ii} \times npoints}{npoints - nvaried}} \quad (2)$$

where ε_{rms} is the root mean square of the fitting residuals, *npoints* is the number of points in the fitting window, and *nvaried* is the number of parameters varied during the fitting.

The fitting uncertainties for single measurements of the BrO VCDs typically vary between 4×10^{12} and 7×10^{12} molecules cm^{-2}, consistently throughout the data record. The uncertainties vary with cross-track positions, from ~7×10^{12} at nadir positions to ~4×10^{12} at edge positions due to the increase of photon path length through the stratosphere. Relatively, the VCD uncertainties typically range between 10-20% of individual BrO VCDs, but could be as low as 5% over BrO hotspots. This is roughly 2-3 times worse that what was achieved from GOME-1 data.

Deleted: The BrO VCD retrieval uncertainties listed in the data product only include spectral fitting errors. Error sources from AMFs (*i.e.*, BrO climatology), atmospheric composition and state (pressure/temperature vertical profiles, total ozone column, *etc.*) and other sources of VCD uncertainty are not included.

The BrO VCD retrieval uncertainties listed in the data product only include random spectral fitting errors. Error sources from AMFs (*i.e.*, BrO climatology), atmospheric composition and state (pressure/temperature vertical profiles, total ozone column, *etc.*) and other sources of VCD uncertainty are not included. We provide here error estimates for these additional error sources.

Uncertainties in the AMFs, used to convert slant to vertical columns, are estimated to be 10% or less except when there is substantially enhanced tropospheric BrO. Hence the total uncertainties of the BrO vertical columns typically range within 15-30%. To estimate the AMF error associated with enhanced tropospheric concentrations we have studied the difference between AMFs calculated using a stratospheric only BrO profile and a stratospheric-tropospheric profile. In this case, we find that the mean absolute difference is 41%. Fig. 4 shows the dependency of the AMFs relative error with respect to wavelength (bottom panel), albedo (middle panel) and VZA (top panel) as a function of the SZA.

We have investigated the sensitivity of OMI BrO VCD with respect to the retrieval window. We studied four wavelength windows including the current operational window (319.0-347.5 nm) version 2 window (323.0-353.5 nm), version 1 (340.0-357.5 nm) and two extra windows exploring the impact of extending the window to shorter wavelengths (310.0-357.5 nm) and reducing it by limiting its extension to wavelengths above 325 nm (325.0-357.5). Table 2 summarizes the results of these studies. The current window results in the most stable retrievals with the smallest number of pixels with negative VCD values. The difference in the mean of the VCDs retrieved using the different fitting windows are always smaller than %50.

Additional sensitivity studies also shown in Table 2 include excluding from the fitting interfering molecules (O_4 and CH_2O), using pre-flight measurements of the slit function or calculating them for each orbit, not including the mean residual (common mode) in the spectral fitting, and changing the order of the closure polynomials. In these experiments, everything else is kept the same as in the operational retrieval. In Table 2, we list the median VCDs and the median uncertainties for BrO for 13 July 2009 orbit number 26564 for each one of these retrieval configurations except for the test of the different orders of the closure polynomials. The results of the polynomial sensitivity test are summarized in Table 3. To study the impact of the slit function variation we have performed the retrieval using both an online slit function modelled as a Gaussian and the preflight instrument function. The mean difference between these two retrievals is 14% (see Table 3) for orbit number 26564.

To study the impact of the radiative transfer effects of the ozone absorption in our retrieval we have adopted the correction method described by Pukite et al., 2010. We find that between 60 degrees south and 60 degrees north the average difference is smaller than 10% with values around 2% near the equator. However, as we move near the poles with solar zenith angles above 60 degrees the differences start to be bigger arriving to mean values around 30%.

Formatted: English (UK)

Formatted: Normal

4 Results and discussions

Comparisons of the OMI OMBRO product with GOME-2 satellite retrievals and remote sensing ground based measurements over Harestua, Norway as well as monthly mean averages illustrate the quality of the retrieval on a global scale. On a local scale, recent scientific studies looking at BrO enhancements in volcanic plumes and over salt lakes are pushing the limits of the current OMBRO setups. In the following sections, we provide details of these comparisons (section 4.1) and discuss OMI OMBRO global distribution (section 4.2) and local enhancements over salt lakes and volcanic plumes observations (section 4.3), and their applicability and strategies to correctly use the publicly available OMBRO product.

4.1 Comparisons with GOME-2 and ground-based observations

To assess the quality of the OMBRO product, we first compared OMI BrO VCDs with BIRA/GOME-2 BrO observations (Theys *et al.*, 2011). GOME-2 and OMI have different orbits: descending orbit with a local equator crossing time (ECT) of 9:30 am for GOME-2 and afternoon ascending orbit with an ECT of 1:45 pm for OMI. To minimize the effects of diurnal variation especially under high SZAs (e.g., McLinden *et al.*, 2006; Sioris *et al.*, 2006) on the comparison, we conduct the comparison using simultaneous nadir overpasses (SNOs) within 2 minutes between GOME-2 and OMI predicted by NOAA National Calibration Center's SNO prediction tool (https://ncc.nesdis.noaa.gov/SNOPredictions). Due to different orbits, all these SNOs occur at high latitudes around 75°S/N. Fig. 5 shows the time series of comparison of individual OMI/GOME-2 BrO retrievals from February 2007 through November 2008. The temporal variation of BrO at the SNO locations is captured similarly by OMI and GOME-2 BrO. The scatter

Deleted: solar zenith angles

Deleted: 4

plot in Fig. 6 quantifies the comparison between OMI and GOME-2 BrO. OMI BrO shows excellent agreement with GOME-2 BrO with a correlation of 0.74, and a mean bias of -0.216 ± 1.13×10^{13} molecules cm^{-2} (mean relative bias of -2.6 ± 22.1%). Considering very different retrieval algorithms including different cross sections and BrO profiles, such a good agreement is remarkable. GOME-2 retrievals use the BrO cross sections of Fleischmann *et al*. (2004) while our BrO retrievals use the BrO cross sections of Wilmouth *et al*. (1999). According to the sensitivity studies by Hendrick *et al.* (2009), using the Fleischmann cross section increases BrO by ~10%. So, accounting for different cross sections, OMI BrO underestimates the GOME-2 BrO by ~10%. In addition, the GOME-2 algorithm uses a residual technique to estimate tropospheric BrO from measured BrO SCDs by subtracting a dynamic estimate of stratospheric BrO climatology driven by O_3 and NO_2 concentrations and by using two different tropospheric BrO profiles depending on surface albedo conditions. This is very different from the approach of using a single BrO profile in the OMI BrO algorithm, and can contribute to some of the BrO differences. Furthermore, additional algorithm uncertainties in both algorithms and different spatial sampling can also cause some differences. Fig. 7 shows the VCDs monthly averages of GOME2 data (green) to OMBRO (black) from February 2007 to December 2009 where the seasonal variations are clearly seen. GOME2 VCDs show an upward trend that is not seen in OMI retrieved VCDs. Our study shows the mean difference for the whole period is 12%, 10%, 17%, and 10% for Alaska, Southern Pacific, Hudson Bay, and Greenland respectively.

We also used ground-based zenith-sky measurements of total column BrO at Harestua, Norway (Hendrick *et al.*, 2007) to estimate the quality of the OMI BrO. We compared daily mean total BrO at Harestua with the mean OMI BrO from individual footprints that contain the location of Harestua site. Fig. 8 shows the time series of the comparison between OMI total BrO and Harestua total BrO from February 2005 through August 2011 with the scatter plot shown in Fig. 9. Ground-based BrO shows an obvious seasonality with high values in the winter/spring and low values in the summer/fall. Such seasonality is well captured by OMI BrO. OMI BrO shows a reasonable good agreement with Harestua BrO with a correlation of 0.46 and a mean bias of $0.12\pm0.76\times10^{13}$ molecules cm^{-2} (mean relative bias of 3.18±16.30%, with respect to individual Harestua BrO). Sihler *et al.* (2012) compared GOME-2 BrO to ground-based observations at Utqiagvik (Barrow) finding the correlation to be weaker (r = 0.3), likely due to both elevated and shallow surface layers

Deleted: 5

Deleted: 6

Deleted: 7

of BrO. However, their correlation between GOME-2 BrO and ground-based measurements at Amundsen, U.S. (r = 0.4) is closer to our correlation here. From the Harestua data, tropospheric BrO typically consists of 15-30% of the total BrO, larger than what we have assumed in the troposphere. The use of a single BrO profile in the OMI BrO algorithm will likely underestimate the actual BrO. Accounting for the uncertainty due to profile shape, OMI BrO will have a larger positive bias relative to Harestua measurements, which can be caused by other algorithm uncertainties and the spatiotemporal differences between OMI and Harestua BrO.

4.2 Global distribution of BrO VCDs

Table 2 shows the median VCD, median uncertainties and the number of negative pixels for the current operational version (V3), V2, and V1. Fig. 10 shows the monthly mean averages for V3 and V3 for the months of February and May of 2008. The differences on the VCD are about 30% in V3 comparing to V2. In comparison with V2 retrieval, the new retrieval (V9) does not show a large increase in the VCD concentrations, especially at the north polar region. The BrO background concentrations over the Pacific Ocean remain the same between the two versions, however, there are more retrieved VCDs.

Formatted: English (UK)

Deleted: 8

Fig. 11 presents the global distribution of monthly mean BrO VCDs for selected months (March, June, September, December) showing BrO seasonality for three different years (2006, 2007 and 2012). BrO typically increases with latitude, with minimal values in the tropics (~2×10^{13} molecules cm^{-2}) and maximum values (~10^{14} molecules cm^{-2}) around polar regions especially in the northern hemisphere winter/spring. In the tropics, BrO shows little seasonality but at higher latitudes in polar regions, BrO displays evident seasonality. The seasonality is different between northern and southern hemispheres. In the northern hemisphere, BrO values are larger in the winter/spring and smaller in the summer/fall, and the enhancement is more widespread during the spring. In the southern hemisphere, BrO values are larger in southern hemispheric spring and summer (i.e., September and January) and smaller in the winter. Such global distribution and seasonal variation are generally consistent with previous satellite measurements (*cf.* Chance, 1998; http://bro.aeronomie.be/level3_monthly.php?cmd=map). BrO in the tropics shows consistent zonal distributions with lower values over land and in the intertropical convergence zone. This

might be related to the impacts of clouds on the retrievals (e.g, BrO below thick clouds cannot be measured, there are uncertainties in the AMF calculation under cloudy conditions) and will be investigated in detail in future studies. The global distribution and seasonal variation are consistent from year to year, but the distributions from different years disclose some interannual variation. For example, BrO values in 2007 are smaller in January but are larger in March compared to those in 2006. Although OMI data since 2009 have been seriously affected by the row anomaly at certain cross-track positions, the monthly mean data derived from good cross-track positions are hardly affected by the row anomaly as shown from the very similar global distribution and seasonality in 2012.

4.3 Salt lakes and volcanic plumes enhancements of BrO

Following recent work by Hörmann et al. (2016) over the Rann of Kutch we have explored the capability of OMBRO to observe similar enhancements in other salt lakes. Fig. 12 shows monthly averaged OMI BrO over the Great Salt Lake for 06/2006, the corresponding surface albedo used in the retrieval, cloud cover (assuming a cloud filter of 40%) as well as the cloud pressure. Over the Great Salt Lake, BrO enhancement occurs predominantly over the lake bed with enhancements of ~5-10×10^{12} molecules cm^{-2} over background values (3-4×10^{13} molecules cm^{-2}). Despite observing these enhancements, the users of OMBRO for these kinds of studies should be aware of three limitations of the current retrieval algorithm. First, the BrO columns assume a mostly stratospheric BrO profile (Figure 3) for the AMF calculation. Second, the OMI derived albedo climatology (Kleipool *et al*. 2008) used in OMBRO has a resolution of 0.5 degrees. At this resolution OMBRO retrievals can have biases given the size of OMI pixels and the inherent sub-pixel albedo variability. Finally, high albedos inherent to salt lakes surface yield abnormally high cloud fractions and low cloud pressures over the salt lakes (Hörmann *et al*., 2016). All these factors should be considered in studies addressing the spatiotemporal distribution of BrO over salt lakes using OMBRO. We have done a preliminary analysis of salt water bodies including the Rann of Kutch. Although this work is not fully complete and will be a separate paper, however, we see maximum BrO VCDs appearing during March–May every year from 2004 – 2015 similar to what was reported by Hörmann et al., 2016. The BrO VCDs we see are around 4.5 x 10^{13} molecules cm^{-2}.

Formatted: Font:Not Bold, No underline, Complex Script Font: Bold

Formatted: Font:Not Bold, No underline, Complex Script Font: Bold

Formatted: Font:Not Bold, No underline, Complex Script Font: Bold, Not Highlight

Formatted: Font:Not Bold, No underline, Complex Script Font: Bold

During our analysis of volcanic eruption scenarios, it was discovered that the currently implemented SO_2 molecular absorption cross sections (Vandaele *et al*., 1994) are a sub-optimum choice (see Fig. 13). Compared to more recent laboratory measurements (Hermans *et al*., 2009; Vandaele *et al*., 2009), the original SO_2 cross sections implemented in OMBRO do not extend over the full BrO fitting window and exhibit the wrong behavior longward of 324 nm, overestimating the most recent measurement by up to a factor of 3. As the correlation between BrO and both SO_2 cross sections are very small (-0.03 for the current SO_2 and 0.11 for the latest SO_2 cross sections) over the spectral range of SO_2 cross sections, interference by SO_2 in BrO retrievals is usually not an issue at average atmospheric SO_2 concentrations, but strong volcanic eruptions will render even small SO_2 absorption features past 333 nm significant. Around 334 nm, the Vandaele *et al*. (2009) data show an SO_2 feature that correlates with BrO absorption when SO_2 concentrations are significantly enhanced. As a consequence of this spectral correlation, SO_2 may be partially aliased as BrO, since the implemented SO_2 cross sections cannot account for it. Fig. 13 presents an example from the 2010 Eyjafjallajökull eruption to show that the BrO retrieval can be affected by the choice of SO_2 cross sections. The next version of the OMBRO public release will be produced using the updated SO_2 absorption cross sections. Until then, caution is advised when using the OMI BrO product during elevated SO_2 conditions. We recommend to use OMBRO product together with the operational OMI SO_2 product (Li *et al.*, 2013) to flag abnormally high BrO retrievals.

The top panels of Fig. 14 show daily average operational BrO VCDs from the eruption of the Eyjafjallajökull volcano on May 5 and 17, 2010, respectively. Enhanced BrO values in excess of 8.0×10^{13} are detected in the vicinity of this volcano (e.g., plume extending southeast ward from the volcano on May 5 and, high BrO over Iceland on May 17). Some of these enhanced BrO values correspond to the locations of enhanced SO_2 as shown from the NASA global SO_2 monitoring website (https://so2.gsfc.nasa.gov/). This enhancement of BrO is not related to the seasonal variation of BrO as no such BrO enhancement is detected over Eyjafjallajökull during May 5-17, 2011 (a year after the eruption), with BrO values of only up to ~5.3×10^{13} molecules cm^{-2} (not shown). The bottom panels of Fig. 14 show the same BrO retrievals using SO_2 cross sections by

Deleted: Following recent work by Hörmann et al. (2016) we have checked the capability of OMBRO to observe similar enhancements in other salt lakes. Fig. 9 shows monthly averaged OMI BrO over the Great Salt Lake for 02/2013. And the Dead Sea for 07/2009. Over the Great Salt Lake, BrO enhancement occurs predominantly over the lake bed with enhancements of ~5-10×10^{12} molecules cm^{-2} over background values (4-4.7×10^{13} molecules cm^{-2}). Over the Dead Sea, the BrO enhancement of 5-8 ×10^{12} molecules cm^{-12} occurs to the South-West, where BrO accumulates at a small hill due to the prevailing north-easterly winds. Despite observing these enhancements, the users of OMBRO for these kinds of studies should be aware of two limitations of the current retrieval. First, the actual BrO enhancement is actually underestimated since we are assuming a mostly stratospheric BrO profile for the AMF. Second, the OMI derived albedo climatology (Kleipool *et al*. 2008) used in OMBRO has a resolution of 0.5 degrees. At this resolution OMBRO retrievals can have biases given the size of OMI pixels and sub-pixel albedo variability not represented in the albedo climatology. We also raise attention to the fact that abnormally high cloud fractions are reported over the salt lakes due to enhanced albedos. All these considerations are important for future studies studying spatiotemporal distribution of BrO over salt lakes.

Deleted: 0

Deleted: 1

Deleted: 1

Deleted: 1

Vandaele et al. (2009). Using the improved SO_2 cross sections increase the BrO over a broader area on both days, supporting that the choice of SO_2 cross sections can affect the BrO retrievals. However, BrO enhancement around the volcano can still clearly be seen with the improved SO_2 cross sections. This suggests that this BrO enhancement is not totally due to aliasing of SO_2 as BrO, but real BrO from the volcanic eruption.

5 Conclusions

This paper describes the current operational OMI BrO retrieval algorithm developed at SAO and the corresponding V3 OMI total BrO (OMBRO) product in detail. The OMI BrO retrieval algorithm is based on nonlinear least-squares direct fitting of radiance spectra in the spectral range 319.0-347.5 nm to obtain vertical column densities (VCDs) directly in one step. Compared to previous versions of two-step algorithms, the fitting window was moved to shorter wavelengths and the spectral range was increased to reduce the fitting uncertainty. Because air mass factors (AMFs) vary significantly with wavelengths as a result of significant variation of ozone absorption, the wavelength and surface albedo dependent AMF, which is precomputed with the Linearized Discrete Ordinate Radiative Transfer (LIDORT) code using a single mostly stratospheric BrO profile, is applied pre-fit to BrO cross sections for direct fitting of VCDs. Prior to the spectral fitting of BrO, wavelength calibration is performed for both irradiance and radiance at each cross-track position and reference spectra are properly prepared at the radiance wavelength grid. Then radiances are modeled from the measured solar irradiance, accounting for rotational Raman scattering, undersampling, attenuation from BrO and interfering gases, and including additive and multiplicative closure polynomials, and the average fitting residual spectrum. To maintain consistency with previous versions, a second fitting of all OMI spectra is performed with unmodified BrO cross sections to derive SCDs and the effective AMFs. Then a destriping step is employed to reduce the cross-track dependent stripes.

Deleted: .05

The uncertainties of BrO VCDs included in the data product include only spectral fitting uncertainties, which typically vary between 4 and 7×10^{12} molecules cm^{-2} (10-20% of BrO VCDs, could be as low as 5% over BrO hotspots), consistent throughout the data record. The uncertainties vary with cross-track positions, from ~7×10^{12} at nadir positions to ~4×10^{12} at edge positions. The

use of single stratospheric BrO profile is another source of uncertainty, overestimating AMFs and therefore underestimating BrO VCDs for conditions with enhanced BrO in the lower troposphere. In addition, the used SO_2 cross sections are a sub-optimum choice and can cause errors in the retrievals under high SO_2 concentrations.

We compared OMI BrO VCDs with BIRA/GOME-2 BrO observations at locations of simultaneous nadir overpasses. OMI BrO shows excellent agreement with GOME-2 BrO with a correlation of 0.74, and a mean bias of $-0.216\pm1.13\times10^{13}$ molecules cm^{-2} (mean relative bias of -2.6 ± 22.1%). We also compared OMI BrO with ground-based zenith-sky measurements of total BrO at Harestua, Norway. This BrO seasonality in Harestua total BrO is well captured by the OMI BrO and OMI BrO shows a reasonable good agreement with a moderate correlation of 0.46 and a small mean bias of $0.12\pm0.76\times10^{13}$ molecules cm^{-2} (mean relative bias of 3.18±16.30%). The global distribution and seasonal variation of OMI BrO are generally consistent with previous satellite measurements. There are small values in the tropics with no much seasonality, and large values at high latitudes with distinct seasonality. And the seasonality is different between the northern and southern hemisphere, with larger values in the hemispheric winter/spring (spring/summer) and smaller values in summer/fall (winter) for the northern (southern) hemisphere. This spatiotemporal variation is generally consistent from year to year and is hardly affected by the row anomaly, but does show some interannual variation. The retrievals show enhanced BrO of $5\text{-}10\times10^{12}$ molecules cm^{-2} over the U.S. Great Salt Lake and also significant enhancement from the eruption of Eyjafjallajökull volcano despite BrO retrievals under high SO_2 conditions can be affected by the current use of a sub-optimal choice of SO_2 cross sections.

Deleted: and the Dead Sea Valley,

Deleted: For the next version, we will update the SO_2 cross sections, test the inclusion of O_2-O_2 cross sections, optimize the spectral fitting including investigating and mitigating the interference of H_2CO on BrO retrieval. We will also improve the AMF calculation accounting for clouds and ozone and consider the use of model-based climatological BrO profiles. The second step of spectral fitting to derive SCDs and effective AMFs will be removed as the effective AMFs can be derived from wavelength dependent AMFs.

Acknowledgements

This study is supported by NASA Atmospheric Composition Program/Aura Science Team (NNX11AE58G) and the Smithsonian Institution. Part of the research was carried out at the Jet Propulsion Laboratory, California Institute of Technology, under a contract with NASA. The Dutch-Finnish OMI instrument is part of the NASA EOS Aura satellite payload. The OMI project

is managed by NIVR and KNMI in the Netherlands. We acknowledge the OMI International Science Team for providing the SAO OMBRO data product used in this study.

References

Abbatt, J. P. D., Thomas, J. L., Abrahamsson, K., Boxe, C., Granfors, A., Jones, A. E., King, M. D., Saiz-Lopez, A., Shepson, P. B., Sodeau, J., Toohey, D. W., Toubin, C., von Glasow, R., Wren, S. N., Yang, X.: Halogen activation via interactions with environmental ice and snow, Atmos. Chem. Phys., 12, 6237–6271, https://doi.org/10.5194/acp-12-6237-2012, 2012.

Acarreta, J.R., De Haan, J.F., and Stammes, P.: Cloud pressure retrieval using the O_2-O_2 absorption band at 477 nm, J. Geophys. Res-Atmos., 109, http://dx.doi.org/10.1029/2003JD003915, 2004.

Aliwell, S.R., Van Roozendael, M., Johnston, P.V., Richter, A., Wagner, T., Arlander, D.W., Burrows, J.P., Fish, D.J., Jones, R.L., Tornkvist, K.K., Lambert, J.-C., Pfeilsticker, K., Pundt, I., Analysis for BrO in zenith-sky spectra: An intercomparison exercise for analysis improvement, J. Geophys. Res., 107(D14), doi:10.1029/2001JD000329, 2002.

Blechschmidt, A.-M., Richter, A., Burrows, J. P., Kaleschke, L., Strong, K., Theys, N., Weber, M., Zhao, X., Zien, A.: An exemplary case of a bromine explosion event linked to cyclone development in the Arctic, Atmos. Chem. Phys., 16, 1773-1788, https://doi.org/10.5194/acp-16-1773-2016, 2016.

Bobrowski, N., Hönninger, G., Galle, B. and Platt, U.: Detection of bromine monoxide in a volcanic plume, Nature, 423, 273-276, 2003.

Bobrowski, N., von Glasow, R., Aiuppa, A., Inguaggiato, S., Louban, I., Ibrahim, O.W., and Platt, U.: Reactive halogen chemistry in volcanic plumes, J. Geophys. Res. Atmos., 112, D06311, doi:10.1029/2006JD007206, 2007.

Bobrowski, N., von Glasow, R., Giuffrida, G.B., Tedesco, D., Aiuppa, A., Yalire, M., Arellano, S., Johansson, M., and Galle, B.: Gas emission strength and evolution of the molar ratio of BrO/SO_2 in the plume of Nyiragongo in comparison to Etna, J. Geophys. Res Atmos., 120, 277-291, doi:10.1002/2013JD0 21069, 2015.

Bracher, A., Lamsal, L.N., Weber, M., Bramstedt, K., Coldewey-Egbers, M., and Burrows, J.P.: Global satellite validation of SCIAMACHY O3 columns with GOME WFDOAS, Atmos. Chem. Phys., 5, 2357-2368, https://doi.org/10.5194/acp-5-2357-2005, 2005.

Buchwitz, M., Rozanov, V.V., and Burrows, J.P.: A near-infrared optimized DOAS method for the fast global retrieval of atmospheric CH_4, CO, CO_2, H_2O, and N_2O total column amounts from SCIAMACHY Envisat-1 nadir radiances, J. Geophys. Res., D105, 15231–15245, 2000.

Burd, Justine A., Peterson, Peter K., Nghiem, Son V., Perovich, Don K., Simpson, William R.: Snowmelt onset hinders bromine monoxide heterogeneous recycling in the Arctic, J. Geophys. Res, Atmos., 122, 8297-8309, 2017.

Burrows, J.P. and Chance, K.V.: Scanning Imaging Absorption Spectrometer for Atmospheric ChartographY, Proc. S.P.I.E., Future European and Japanese Remote Sensing Sensors and Programs, 1490 146-154, 1991.

Caspar, C. and Chance, K.: GOME wavelength calibration using solar and atmospheric spectra, in: Third ERS Symposium on Space at the service of our Environment, edited by: Guyenne, T.-D. and Danesy, D., Vol. 414 of ESA Special Publication, p. 609, 1997.

Chan Miller, C., González Abad, G., Wang, H., Liu, X., Kurosu, T., Jacob, D.J., and Chance, K.: Glyoxal retrieval from the Ozone Monitoring Instrument, Atmos. Meas. Tech., 7, 3891-3907, 2014.

Chan Miller, C., Jacob, D.J., González Abad, G., and Chance, K.: Hotspot of glyoxal over the Pearl River Delta seen from the OMI satellite instrument: Implications for emissions of aromatic hydrocarbons, Atmos. Chem. Phys., 16, 4631-4639, doi:10.5194/acp-16-4631-2016, 2016.

Chance, K. and Kurucz, R., An improved high-resolution solar reference spectrum for earth's atmosphere measurements in the ultraviolet, visible, and near infrared, J. Quant. Spectrosc. Radiat. Transfer, 111, 1289–1295, doi:10.1016/j.jqsrt.2010.01.036, 2010.

Chance, K., and Orphal, J.: Revised ultraviolet absorption cross sections of H_2CO for the HITRAN database, J. Quant. Spectrosc. Radiat. Transfer, 112, 1509-1510, doi:10.1016/j.jqsrt.2011.02.002, 2011.

Chance, K., and Kurucz, R.L.: An improved high-resolution solar reference spectrum for Earth's atmosphere measurements in the ultraviolet, visible, and near infrared, J. Quant. Spectrosc. Radiat. Transfer, 111, 1289-1295, 2010.

Chance, K., Kurosu, T.P., and Sioris, C.E.: Undersampling correction for array-detector based satellite spectrometers, Appl. Opt., 44, 1296-1304, 2005.

Chance, K., Palmer, P.I., Spurr, R.J.D., Martin, R.V., Kurosu, T.P., and Jacob, D. J.: Satellite observations of formaldehyde over North America from GOME, Geophys. Res. Lett., 27, 3461–3464, doi:10.1029/2000GL011857, 2000.

Chance, K.: Analysis of BrO measurements from the Global Ozone Monitoring Experiment, Geophys. Res. Lett., 25, 3335-3338, 1998.

Chance, K.: Spectroscopic Measurements of Tropospheric Composition from Satellite Measurements in the Ultraviolet and Visible: Steps Toward Continuous Pollution Monitoring from Space, in "Remote Sensing of the Atmosphere for Environmental Security," Eds. A. Perrin, N. Ben Sari-Zizi, and J. Demaison, NATO Security through Science Series, ISBN: 1-4020-5089-5, Springer, pp. 1-25, 2006.

Chance, K.V. and Spurr, R.J.D.: Ring effect studies: Rayleigh scattering, including molecular parameters for rotational Raman scattering, and the Fraunhofer spectrum, Appl. Opt., 36, 5224-5230, doi:10.1364/AO.36.005224, 1997.

Chance, K.V., Burrows, J.P., and Schneider, W.: Retrieval and molecule sensitivity studies for the Global Ozone Monitoring Experiment and the SCanning Imaging Absorption spectroMeter for Atmospheric CHartographY, Proc. S.P.I.E., Remote Sensing of Atmospheric Chemistry, 1491, 151-165, 1991.

Choi, S., Wang, Y., Salawitch, R.J., Canty, T., Joiner, J., Zeng, T., Kurosu, T.P., Chance, K., Richter, A., Huey, L.G., Liao, J., Neuman, J.A., Nowak, J.B., Dibb, J.E., Weinheimer, A.J., Diskin, G., Ryerson, T.B., da Silva, A., and Curry, J.: Analysis of satellite-derived Arctic tropospheric BrO columns in conjunction with aircraft measurements during ARCTAS and ARCPAC, Atmos. Chem. Phys., 12, 1255-1285, doi: 10.5194/acp-12-1255-2012, 2012.

Coldewey-Egbers, M., Weber, M., Lamsal, L.N., de Beek, R., Buchwitz, M., and Burrows, J.P.: Total ozone retrieval from GOME UV spectral data using the weighting function DOAS approach, Atmos. Chem. Phys., 5, 1015-1025, https://doi.org/10.5194/acp-5-1015-2005, 2005.

De Smedt, I., Van Roozendael, M., Stavrakou, T., Müller, J.- F., Lerot, C., Theys, N., Valks, P., Hao, N., and van der A, R. (2012). Improved retrieval of global tropospheric formaldehyde columns from GOME-2/MetOp-A addressing noise reduction and instrumental degradation issues. Atmospheric Measurement Techniques, 5(11):2933–2949.

De Smedt, I., Stavrakou, T., Hendrick, F., Danckaert, T., Vlemmix, T., Pinardi, G., Theys, N., Lerot, C., Gielen, C., Vigouroux, C., Hermans, C., Fayt, C., Veefkind, P., Müller, J.-F., and Van Roozendael, M.: Diurnal, seasonal and long-term variations of global formaldehyde columns inferred from combined OMI and GOME-2 observations, Atmos. Chem. Phys., 15, 12519–12545, https://doi.org/10.5194/acp-15-12519-2015, 2015.

Dirksen, R., Dobber, M., Voors, R., and Levelt, P.: Prelaunch characterization of the Ozone Monitoring Instrument transfer function in the spectral domain, Appl. Opt., 45, 3972-3981, 2006.

Fleischmann, O.C., Hartmann, M., Burrows, J.P., and Orphal, J.: New ultraviolet absorption cross sections of BrO at atmospheric temperatures measured by time-windowing Fourier transform spectroscopy, J. Photochem. Photobiol. A., 168, 117–132, doi:10.1016/j.jphotochem.2004.03.026, 2004.

González Abad, G., Liu, X., Chance, K., Wang, H., Kurosu, T.P., and Suleiman, R.: Updated Smithsonian Astrophysical Observatory Ozone Monitoring Instrument (SAO OMI) formaldehyde retrieval, Atmos. Meas. Tech., 8, 19-32, doi:10.5194/amt-8-19-2015, 2015.

Greenblatt, G. D., Orlando, J. J., Burkholder, J. B., and Ravishankara, A. R. (1990). Absorption measurements of oxygen between 330 and 1140 nm. J. Geophys. Res., 95:18577–18582.

Frieß, U., Sihler, H., Sander, R., PöHler, D., Yilmaz, S., Platt, U.: The vertical distribution of BrO and aerosols in the Arctic: Measurements by active and passive differential optical absorption spectroscopy, J. Geophys. Res., 116, D00R04, doi: 10.1029/2011JD015938, 2011.

Hausmann, M., Platt, U.: Spectroscopic measurement of bromine oxide and ozone in the high Arctic during Polar Sunrise Experiment 1992, J. Geophys. Res., D12, 25399-25413,1994.

Hebestreit, K., Stutz, J., Rosen, D., Matveiv, V., Peleg, M., Luria, M., Platt, U.: DOAS Measurements of Tropospheric Bromine Oxide in Mid-Latitudes, Science, 283, 5398, 55, doi: 10.1126/science.283.5398.55, 1999.

Hendrick, F., Van Roozendael, M., Chipperfield, M.P., Dorf, M., Goutail, F., Yang, X., Fayt, C., Hermans, C., Pfeilsticker, K., Pommereau, J.-P., Pyle, J.A., Theys, N., and De Maziére, M. Retrieval of stratospheric and tropospheric BrO profiles and columns using ground-based zenith-sky DOAS observations at Harestua, 60° N, Atmos. Chem. Phys., 7, 4869-4885, https://doi.org/10.5194/acp-7-4869-2007, 2007.

Hendrick, F., Johnston, P.V., De Mazière, M., Fayt, C., Hermans, C., Kreher, K., Theys, N., Thomas, A., and Van Roozendael, M.: One-decade trend analysis of stratospheric BrO over Harestua (60° N) and Lauder (45° S) reveals a decline, Geophys. Res. Lett., 35, L14801, doi:10.1029/2008gl034154, 2008.

Hendrick, F., Rozanov, A., Johnston, P.V., Bovensmann, H., De Mazière, M., Fayt, C., Hermans, C., Kreher, K., Lotz, W., Sinnhuber, B.-M., Theys, N., Thomas, A., Burrows, J.P., and Van Roozendael, M.: Multi-year comparison of stratospheric BrO vertical profiles retrieved from SCIAMACHY limb and ground-based UV-visible measurements, Atmos. Meas. Tech., 2, 273-285, https://doi.org/10.5194/amt-2-273-2009, 2009.

Hermans, C., Vandaele, A.C., and Fally, S.: Fourier transform measurements of SO_2 absorption cross sections: I. Temperature dependence in the 24 000 - 29 000 cm-1 (345-420 nm) region, J. Quant. Spectrosc. Radiat. Transfer, 110, 756-765, 2009.

Hermans, C., Vandaele, A.C., Fally, S., Carleer, M., Colin, R., Coquart, B., Jenouvrier, A., and Merienne, M.-F.: Absorption cross sections of the collision-induced bands of oxygen from the UV to the NIR, NATO Advanced Research Workshop on Weakly Interacting Molecular Pairs: Unconventional Absorbers of Radiation in the Atmosphere, Eds. C. Camy-Peyret and A. Vigasin, Kluwer Academic Publ., NATO Meeting series, ISBN: 1-4020-1596-8, 193-202, 2003.

Hermans, C., Vandaele, A. C., Carleer, M., Fally, S., Colin, R., Jenouvrier, A., Coquart, B., and Mérienne, M.-F. (1999). Absorption cross-sections of atmospheric constituents: NO2, O2, and H2O. Environ. Sci. & Pollut. Res., 6(3):151–158.

Holla, R., Schmitt, S., Frieß, U., Pöhler, D., Zingler, J., Corsmeier, U., Platt, U.: Vertical distribution of BrO in the boundary layer at the Dead Sea, Environ. Chem., 10.1071/EN14224, 12, 4, 438-460, 2015.

Hollwedel, J., Wenig, M., Beirle, S., Kraus, S., Kühl, S., Wilms-Grabe, W., Platt, U., and Wagner, T.: Year-to-year variations of spring time polar tropospheric BrO as seen by GOME, Adv. Space Res., 34, 4, 804-808, 2004.

Hörmann, C., Sihler, H., Bobrowski, N., Beirle, S., Penning de Vries, M., Platt, U., Wagner, T.: Systematic investigation of bromine monoxide in volcanic plumes from space by using the GOME-2 instrument, Atmos. Chem. Phys., 13, 4749-4781, https://doi.org/10.5194/acp-13-4749-2013, 2013.

Hörmann, C., Sihler, H., Beirle, S., Penning de Vries, M., Platt, U., and Wagner, T.: Seasonal variation of tropospheric bromine monoxide over the Rann of Kutch salt marsh seen from space, Atmos. Chem. Phys., 16, 13015-13034, doi:10.5194/acp-16-13015-2016, 2016.

Huang, G., Liu, X., Chance, K., Yang, K., Bhartia, P. K.,Cai, Z., Allaart, M., Ancellet, G., Calpini, B., Coetzee, G.J.R., Cuevas-Agulló, E., Cupeiro, M., De Backer, H., Dubey, M.K., Fuelberg, H.E., Fujiwara, M., Godin-Beekmann, S., Hall, T.J., Johnson, B., Joseph, E., Kivi, R., Kois, B., Komala, N., König-Langlo, G., Laneve, G., Leblanc, T., Marchand, M., Minschwaner, K.R., Morris, G., Newchurch, M.J., Ogino, S.-Y., Ohkawara, N., Piters, A.J.M., Posny, F., Querel, R., Scheele, R., Schmidlin, F.J., Schnell, R.C., Schrems, O., Selkirk, H., Shiotani, M., Skrivánková, P., Stübi, R., Taha, G., Tarasick, D.W., Thompson, A. M.,Thouret, V., Tully, M. B., Van Malderen, R., Vömel,

H., von der Gathen, P., Witte, J.C., and Yela, M.: Validation of 10-year SAO OMI Ozone Profile (PROFOZ) product using ozonesonde observations, Atmos. Meas. Tech., 10, 2455-2475, https://doi.org/10.5194/amt-10-2455-2017, 2017.

Huang, G., Liu, X., Chance, K., Yang, K., and Cai, Z.: Validation of 10-year SAO OMI Ozone Profile (PROFOZ) Product Using Aura MLS Measurements, Atmos. Meas. Tech., 11, 17-32, https://doi.org/10.5194/amt-11-17-2018, 2018.

Kinnison, D., Tilmes, S., Levelt, P.F. Dirksen, R., Dobber, M., Voors, R., and Levelt, P.: Prelaunch characterization of the Ozone Monitoring Instrument transfer function in the spectral domain, Appl. Opt., 45, 3972–3981, doi:10.1364/AO.45.003972, 2006.

Kleipool, Q.L., Dobber, M.R., de Haan, J.F., and Levelt, P.F.: Earth surface reflectance climatology from 3 years of OMI data, J. Geophys. Res., 113, D18308, doi:10.1029/2008JD010290, 2008.

Kromminga, H., Voigt, S., Orphal, J., and Burrows, J.P.: The temperature dependence (213–293 K) of the absorption cross-sections of OClO in the 340–450 nm region measured by Fourier-transform spectroscopy, J. Photochem. Photobiol. A,157, 149-160, 2003.

Kroon, M., de Haan, J.F., Veefkind, J.P., Froidevaux, L., Wang, R., Kivi, R., and Hakkarainen, J.J., Validation of operational ozone profiles from the Ozone Monitoring Instrument, J. Geophys. Res., 116, D18305, doi:10.1029/2010JD015100, 2011.

Kühl, S., Pukite, J., Deutschmann, T., Platt, U., and Wagner, T.: SCIAMACHY limb measurements of NO_2, BrO and OClO. Retrieval of vertical profiles: algorithm, first results, sensitivity and comparison studies, Adv. Space Res., 42, 1747-1764, 2008.

Kurosu, T.P., Chance, K., and Sioris, C.E.: Preliminary results for HCHO and BrO from the EOS-Aura Ozone Monitoring Instrument, in Proc. SPIE 5652, Passive Optical Remote Sensing of the Atmosphere and Clouds IV, doi: 10.1117/12.578606 2004.

Lee, C., Richter, A., Weber, M., and Burrows, J.P.: SO_2 Retrieval from SCIAMACHY using the Weighting Function DOAS (WFDOAS) technique: comparison with Standard DOAS retrieval, Atmos. Chem. Phys., 8, 6137–6145, 2008.

Levelt, P.F., van den Oord, G.H.J., Dobber, M.R., Mälkki, A., Visser, H., de Vries, J., Stammes, P., Lundell, J., and Saari, H.: The Ozone Monitoring Instrument, IEEE Trans. Geo. Rem. Sens., 44, 1093-1101, doi:10.1109/TGRS.2006.87233, 2006.

Li, C., Joiner, J., Krotkov, N. A., and Bhartia, P. K.: A fast and sensitive new satellite SO2 retrieval algorithm based on principal component analysis: Application to the ozone monitoring instrument, Geophys. Res. Lett., 40, 6314–6318, https://doi.org/10.1002/2013GL058134, 2013.

J. Liao, H. Sihler, L. G. Huey, J. A. Neuman, D. J. Tanner, U. Friess, U. Platt, F. M. Flocke, J. J. Orlando, P. B. Shepson, H. J. Beine, A. J. Weinheimer, S. J. Sjostedt, J. B. Nowak, D. J. Knapp, R. M. Staebler, W. Zheng, R. Sander, S. R. Hall, and K. Ullmann: A comparison of Arctic BrO measurements by chemical ionization mass spectrometry and long path-differential optical absorption spectroscopy, J. Geophys. Res.-Atmos., 116, D00r02, doi:10.1029/2010jd014788, 2011.

Liao, J., Huey, L. G., Tanner, D. J., Flocke, F. M., Orlando, J. J., Neuman, J. A., Nowak, J. B., Weinheimer, A. J., Hall, S. R., Smith, J. N., Fried, A., Staebler, R. M., Wang, Y., Koo, J.-H., Cantrell, C. A., Weibring, P., Walega, J., Knapp, D. J., Shepson, P. B., Stephens, C. R.: Observations of inorganic bromine (HOBr, BrO, and Br2) speciation at Barrow, Alaska, in spring 2009, J. Geophys. Res. Atmos., 117, DOI:10.1029/2011JD016641, 2012

Lindström, P., and Wedin, P.-Å.: Gauss-Newton Based Algorithms for Constrained Nonlinear Least Squares Problems, Tech. Rep. UMINF-901.87, University of Umeå, 1987 (software and report available at http://plato.asu.edu/sub/nonlsq.html).

Liu, X., Bhartia, P.K., Chance, K., Spurr, R.J.D., and Kurosu, T.P.: Ozone profile retrievals from the Ozone Monitoring Instrument, Atmos. Chem. Phys. 10, 2521-2537, 2010.

Malicet, J., Daumont, D., Charbonnier, J., Parisse, C., Chakir, A., and Brion, J.: Ozone UV spectroscopy. II. Absorption cross sections and temperature dependence, J. Atmos. Chem., 21, 263-273, doi:10.1007/BF00696758, 1995.

Marquardt, D.L.: An algorithm for least-squares estimation of non-linear parameters, J. Soc. Indust. Appl. Math. 2, 431-441, 1963.

Martin, R.V., Sioris, C.E., Chance, K., Ryerson, T.B., Bertram, T.H., Wooldridge, P.J., Cohen, R.C., Neuman, J.A., Swanson, A., and Flocke, F.M.: Evaluation of space-based constraints on global nitrogen oxide emissions with regional aircraft measurements over and downwind of eastern North America, J. Geophys. Res., 111, D15308, doi:10.1029/2005JD006680, 2006.

Matveev, V., Mordechai, P., Rosen, D., Tov-Alper, D.S., Hebestreit, K., Stutz, J., Platt, U., Blake, D., and Luria, M.: Bromine oxide-ozone interaction over the Dead Sea, J. Geophys. Res. Atmos., 106, 10375-10387, 2001.

Deleted: Liao, J., Huey, L. G., Scheuer, E., Dibb, J. E., Stickel, R. E., Tanner, D. J., Neuman, J. A., Nowak, J. B., Choi, S., Wang, Y., Salawitch, R. J., Canty, T., Chance, K., Kurosu, T., Suleiman, R., Weinheimer, A. J., Shetter, R. E., Fried, A., Brune, W., Anderson, B., Zhang, X., Chen, G., Crawford, J., Hecobian, A., Ingall, E. D.: Characterization of soluble bromide measurements and a case study of BrO observations during ARCTAS, Atmos. Chem. Phys., 11, 26999-27030, https://doi.org/10.5194/acp-12-1327-2012, 2012.

McLinden, C. A., Haley, C. S., and Sioris, C. E., Diurnal effects in limb scatter observations, J. Geophys. Res., 111, D14302, doi:10.1029/2005JD006628, 2006.

OMI Algorithm Theoretical Basis Document, Volume IV, OMI Trace Gas Algorithms, K. Chance, Ed., ATBD-OMI-04, Version 2.0, 2002.

Peterson, P. K., Simpson, W. R., and Nghiem, S. V.: Variability of bromine monoxide at Barrow, Alaska, over four halogen activation (March–May) seasons and at two on-ice locations, J. Geophys. Res.-Atmos., 121, 1381–1396, doi:10.1002/2015JD024094, 2016.

Peterson, Peter K., Simpson, William R., Nghiem, Son V.: Variability of bromine monoxide at Barrow, Alaska, over four halogen activation (March-May) seasons and at two on-ice locations, J. Geophys. Res. Atmos., 121, 1381-1396, 2016.

Platt, U.: Differential optical absorption spectroscopy (DOAS), Chem. Anal. Series, **127**, 27-83, 1994.

Platt, U. and Wagner, T.: Satellite mapping of enhanced BrO concentrations in the troposphere, Nature, 395, 6701, 486-490, 1998.

Press, W.H., Flannery, B.P., Teukolsky, S.A., and Vetterling, W.T.: Numerical Recipes, ISBN 0-521-30811-9, Cambridge University Press, 1986.

Richter, A., Begoin, M., Hilboll, A., and Burrows, J.P., An improved NO_2 retrieval for the GOME-2 satellite instrument, Atmos. Meas. Tech., 4, 1147–1159, 2011 doi:10.5194/amt-4-1147-2011.

Puk¯ite, Janis, J., Kühl, S., Deutschmann, T., Platt, U., and Wagner, T. (2010). Extending differential optical absorption spectroscopy for limb measurements in the UV. Atmospheric Measurement Techniques, 3(3):631–653.

Richter, A., Wittrock, F., Eisinger, M., and Burrows, J.P., GOME observations of tropospheric BrO in northern hemispheric spring and summer 1997, Geophys. Res. Lett., 25, 14, 2683-2686, 1998.

Rodgers, C.D.: Inverse methods for atmospheric sounding, World Scientific, 2000.

Salawitch, R.J., Canty, T., Kurosu, T., Chance, K., Q. Liang A. da Silva S. Pawson J. E. Nielsen J. M. Rodriguez P. K. Bhartia X. Liu L. G. Huey J. Liao R. E. Stickel D. J. Tanner J. E. Dibb W. R. Simpson D. Donohoue A. Weinheimer F. Flocke D. Knapp D. Montzka J. A. Neuman J. B. Nowak T. B. Ryerson S. Oltmans D. R. Blake E. L. Atlas D. E. Kinnison S. Tilmes L. L. Pan F. Hendrick M. Van Roozendael K. Kreher P. V. Johnston R. S. Gao B. Johnson T. P. Bui

G. Chen R. B. Pierce J. H. Crawford D. J. Jacob: A new interpretation of total column BrO during Arctic spring, Geophys. Res. Lett., 37, L21805, doi:10.1029/2010GL043798, 2010.

Salawitch, R.J., Weinstein, D.K., Kovalenko, L.J., Sioris, C.E., Wennberg, P.O., Chance, K., Ko, M.K.W., and McLinden, C.A.: Sensitivity of ozone to bromine in the lower stratosphere, Geophys. Res. Lett., 32, 5, L05811, doi:10.1029/2004GL021504, 2005.

Schofield, R., Connor, B.J., Kreher, K., Johnston, P.V., and Rodgers, C.D.: The retrieval of profile and chemical information from groundbased UV-visible spectroscopic measurements, J. Quant. Spectrosc. Radiat. Transfer, 86, 115 – 131, 2004a.

Schofield, R., Johnston, P.V., Thomas, A., Kreher, K., Connor, B.J., Wood, S., Shooter, D., Chipperfield, M P., Richter, A., von Glasow, R., and Rodgers, C.D.: Tropospheric and stratospheric BrO columns over Arrival Heights, Antarctica, 2002, J. Geophys. Res., 111, D22310, doi:10.1029/2005JD007022, 2006.

Schofield, R., Kreher, K., Connor, B.J., Johnston, P.V., Thomas, A., Shooter, D. Chipperfield, M.P., Rodgers, C.D., and Mount, G.H.: Retrieved tropospheric and stratospheric BrO columns over Lauder, New Zealand, J. Geophys. Res., 109, D14304, doi:10.1029/2003JD00446, 2004b.

Simpson, W.R., Alvarez-Aviles, L., Douglas, T.A., Sturm, M., and Domine, F.: Halogens in the coastal snow pack near Barrow, Alaska: Evidence for active bromine air-snow chemistry during springtime, Geophys. Res. Lett., 32, L04811, doi:10.1029/2004GL021748, 2005.

Sihler, H., Platt, U., Beirle, S., Marbach, T., Kühl, S., Dörner, S., Verschaeve, J., Frieß, U., Pöhler, D., Vogel, L., Sander, R., Wagner, T.: Tropospheric BrO column densities in the Arctic derived from satellite: retrieval and comparison to ground-based measurements, Atmos. Meas. Tech., 5, 2779-2807, https://doi.org/10.5194/amt-5-2779-2012, 2012.

Simpson, W. R., von Glasow, R., Riedel, K., Anderson, P., Ariya, P., Bottenheim, J., Burrows, J., Carpenter, L. J., Frieß, U., Goodsite, M. E., Heard, D., Hutterli, M., Jacobi, H.-W., Kaleschke, L., Neff, B., Plane, J., Platt, U., Richter, A., Roscoe, H., Sander, R., Shepson, P., Sodeau, J., Steffen, A., Wagner, T., Wolff, E.: Halogens and their role in polar boundary-layer ozone depletion, Atmos. Chem. Phys., 7, 4375-4418, https://doi.org/10.5194/acp-7-4375-2007, 2007.

Sioris, C.E., Kovalenko, L.J., McLinden, C.A., Salawitch, R.J., Van Roozendael, M., Goutail, F., Dorf M., Pfeilsticker, K., Chance, K., von Savigny, C., Liu, X., Kurosu, T.P., Pommereau, J.-P., Bosch, H., and Frerick, J., Latitudinal and vertical distribution of bromine monoxide in the lower

stratosphere from Scanning Imaging Absorption Spectrometer for Atmospheric Chartography limb scattering measurements, J. Geophys. Res., 111, D14301, doi:10.1029/2005JD006479, 2006.

Slijkhuis, S., von Bargen, A., Thomas, W., and Chance, K.: Calculation of undersampling correction spectra for DOAS spectral fitting, in Proceedings of the European Symposium on Atmospheric Measurements from Space, 563–569, 1999.

Spurr, R.J.D.: VLIDORT: A linearized pseudo-spherical vector discrete ordinate radiative transfer code for forward model and retrieval studies in multilayer multiple scattering media, J. Quant. Spectrosc. Radiat. Transfer, 102, 316-342, doi:10.1016/j/jqsrt.2006.05.005, 2006.

Stutz, J., Ackermann, Ralf, Fast, Jerome D., Barrie, Leonard: Atmospheric reactive chlorine and bromine at the Great Salt Lake, Utah, Geophys. Res. Lett., 29, 18-1, doi: 10.1029/2002GL014812, 2002.

Stutz, J., Thomas, J. L., Hurlock, S. C., Schneider, M., von Glasow, R., Piot, M., Gorham, K., Burkhart, J. F., Ziemba, L., Dibb, J. E., Lefer, B. L.: Longpath DOAS observations of surface BrO at Summit, Greenland, Atmos. Chem. Phys., 11, 9899-9910, https://doi.org/10.5194/acp-11-9899-2011, 2011.

Sun, K., Liu, X., Huang, G., González Abad, G., Cai, Z., Chance, K., and Yang, K. (2017). Deriving the slit functions from omi solar observations and its implications for ozone-profile retrieval. Atmospheric Measurement Techniques, 10(10):3677–3695.

Thalman, R. and Volkamer, R. (2013). Temperature dependent absorption cross-sections of O2–O2 collision pairs between 340 and 630 nm and at atmospherically relevant pressure. Physical Chemistry Chemical Physics, 15(37):15371–15381.

Tas, E., Peleg, M., Matveev, V., Zingler, J., Luria, M.: Frequency and extent of bromine oxide formation over the Dead Sea, J. Geophys. Res., D11304, doi:10.1029/2004JD005665, 2005.

Theys, N., Van Roozendael, M., Dils, B., Hendrick, F., Hao, N., and De Mazière, M.: First satellite detection of volcanic bromine monoxide emission after the Kasatochi eruption, Geophys. Res. Lett., 36, L03809, doi:10.1029/2008GL036552, 2009.

Theys, N., Van Roozendael, M., Hendrick, F., Yang, X., De Smedt, I., Richter, A., Begoin, M., Errera, Q., Johnston, P.V., Kreher, K., and De Mazière, M.: Global observations of tropospheric BrO columns using GOME-2 satellite data, Atmos. Chem. Phys., 11, 1791-1811, https://doi.org/10.5194/acp-11-1791-2011, 2011.

K. Toyota, J. C. McConnell, A. Lupu, L. Neary, C. A. McLinden, A. Richter, R. Kwok, K. Semeniuk, J. W. Kaminski, S.-L. Gong, J. Jarosz, M. P. Chipperfield, and C. E. Sioris, Atmos. Chem. Phys., 11, 3949-3979, doi:10.5194/acp-11-3949-2011, 2011.

Vandaele, A.C., Simon, P.C., Guilmot, J.M., Carleer, M., Colin, R.: SO2 Absorption Cross Section measurement in the UV using a Fourier Transform Spectrometer. J. Geophys. Res., 99, 25599-25605, 1994.

Vandaele, A.C., Hermans, C., Simon, P.C., Carleer, M., Colin, R., Fally, S., Mérienne, M.F., Jenouvrier, A., and Coquart, B.: Measurements of the NO_2 absorption cross sections from 42000 cm^{-1} to 10000 cm^{-1} (238-1000 nm) at 220 K and 294 K, J. Quant. Spectrosc. Radiat. Transfer, 59, 171-184, 1998.

Vandaele, A.C., Hermans, C., and Fally, S.: Fourier Transform measurements of SO_2 absorption cross sections: II. Temperature dependence in the 29 000 - 44 000 cm^{-1} (227-345 nm) region, J. Quant. Spectrosc. Radiat. Transfer, 110, 2115-2126, 2009.

Veihelmann, B. and Kleipool, Q.: Reducing Along-Track Stripes in OMI-Level 2 Products, Technical report TN-OMIE-KNMI-785, KNMI, available at http: //disc.sci.gsfc.nasa.gov/Aura/data-holdings/OMI/documents/ v003/RD08_TN785_i1_Reducing_AlongTrack_Stripes.pdf, 2006.

von Glasow, R., von Kuhlmann, R., Lawrence, M.G., Platt, U., and Crutzen, P.J.: Impact of reactive bromine chemistry in the troposphere, Atmos. Chem. Phys., 4, 2481-2497, 2004.

Wang, H., Liu, X., Chance, K., González Abad, G., and Chan Miller, C.: Water vapor retrieval from OMI visible spectra, Atmos. Meas. Tech., 7, 1901-1913, 2014.

Wang, H., González Abad, G., Liu, X., and Chance, K.: Validation of OMI total column water vapor product, Atmos. Chem. Phys., 16, 11379-11393, doi:10.5194/acp-16-11379-2016, 2016.

Weber, M., Lamsal, L.N., Coldewey-Egbers, M., Bramstedt, K., and Burrows, J.P.: Pole-to-pole validation of GOME WFDOAS total ozone with groundbased data, Atmos. Chem. Phys., 5, 1341-1355, https://doi.org/10.5194/acp-5-1341-2005, 2005.

Wilmouth, D.M., Hanisco, T.F., Donahue, N.M, and Anderson, J.G.: Fourier transform ultraviolet spectroscopy of the $A^2\Pi_{3/2} \leftarrow X^2\Pi_{3/2}$ transition of BrO, J. Phys. Chem. A, 103, 8935-8945, 1999.

Yung, Y.L., Pinto, J.P., Watson, R.T., and Sander,S. P.: Atmospheric bromine and ozone perturbations in the lower stratosphere, J. Atmos. Sci., 37, 2, 339, 1980.

Zhao, X., Strong, K., Adams, C., Schofield, R., Yang, X., Richter, A., Friess, U., Blechschmidt, A.-M., Koo, J.-H.: A case study of a transported bromine explosion event in the Canadian high arctic, J. Geophys. Res. Atmos., 121, 457-477, doi: 10.1002/2015JD023711, 2015.

Table 1. Fitting window and parameters used to derive BrO vertical column densities

Parameter	Description/value
Fitting window	319.0 - 347.5 nm
Baseline polynomial	4th order
Scaling polynomial	4th order
Instrument slit function	Hyper-parameterization of pre-flight measurements, Dirksen *et al*., 2006
Wavelength calibration	Spectral shift (no squeeze)
Solar reference spectrum	Chance and Kurucz, 2010
BrO cross sections	Wilmouth *et al*., 1999, 228K
H_2CO cross sections	Chance and Orphal, 2011, 300K
O_3 cross sections	Malicet *et al*., 1995, 218K, 295K
NO_2 cross sections	Vandaele *et al*., 1998, 220K
SO_2 cross sections	Vandaele et al., 1994, 295K[1] Hermans *et al.*, 2009; Vandaele *et al.*, 2009, 295K[2]
OClO cross sections	Kromminga *et al*., 2003, 213K
Molecular Ring cross sections	Chance and Spurr, 1997
Undersampling correction	Computed on-line, Chance *et al*., 2005
Residual (common mode) spectrum	Computed on-line between 30°N and 30°S

1. Used in the current operational algorithm.
2. Used for testing sensitivity to SO_2 cross sections and will be used in the next version.

Formatted Table

Table 2. Error analysis studies.

Description	Median VCD (Molec. cm^{-2})	Median uncertainty (Molec. cm^{-2})	Number of negatives
Operational (V3)	3.89×10^{13}	7.85×10^{12}	1222
323.0 - 353.5 nm (V2)	2.69×10^{13}	1.01×10^{13}	4393
340.0 – 357.5 nm (V1)	2.48×10^{13}	1.29×10^{13}	9390
310.0 - 357.5 nm	1.91×10^{13}	6.83×10^{12}	7372
325.0 - 357.5 nm	3.10×10^{13}	8.75×10^{12}	3107
With O_2-O_2	3.57×10^{13}	8.65×10^{12}	1265
Online slit function	5.00×10^{13}	7.92×10^{12}	1003
Without common mode	3.72×10^{13}	1.11×10^{13}	2093
Without HCHO	2.53×10^{13}	6.93×10^{12}	1703

Comment [RMS1]: Changed them to V3, V2, V1 and out them in order.

Table 3. Summary of different errors sources in the BrO vertical column.

Formatted: Font:Bold, German

Error source	Type	Parameter uncertainty	Averaged uncertainty on BrO VCD	Evaluation method - reference
Measurement noise random	Random	S/N 500 - 1000	4-7x10^{12} molec. cm^{-2}	Error propagation;
HCHO	Systematic	Based on literature reported error estimates	5%	Chance and Orphal, 2011, 300K
O_3			2%	Malicet et al., 1995, 218K, 295K
BrO			8%	Wilmouth et al., 1999, 228K
NO_2			3%	Vandaele et al., 1998, 220K
SO_2			5%	Vandaele et al., 1994, 295K
OClO			5%	Kromminga et al., 2003, 213K
Ring			5%	Chance and Spurr, 1997
Offset order	Systematic	Vary polynomial order	10%	Sensitivity analysis
Polynomial order	Systematic	Vary polynomial order	10%	
Instrumental slit function and wavelength calibration	Systematic	Preflight and online slit function	28%	
Wavelength interval	Systematic	Varying fitting window	50%	

Figures and Figure Captions

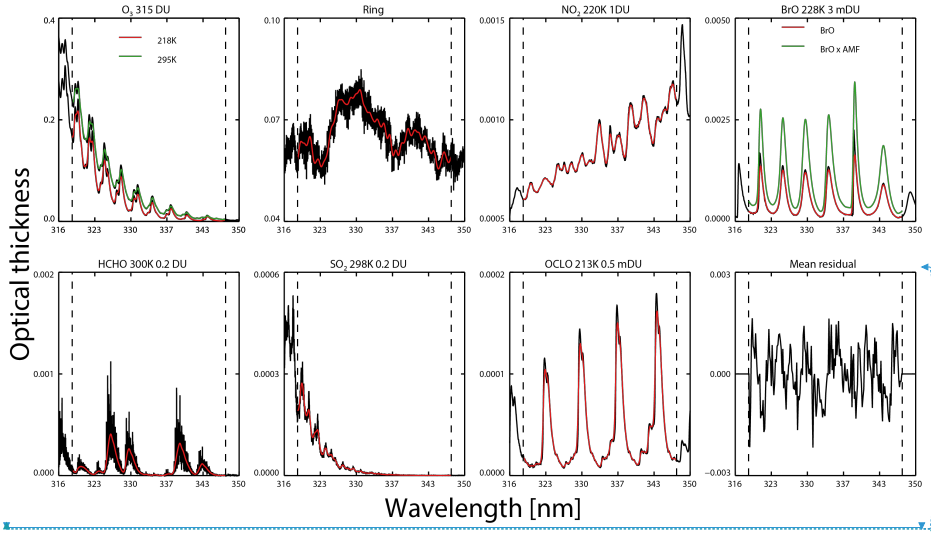

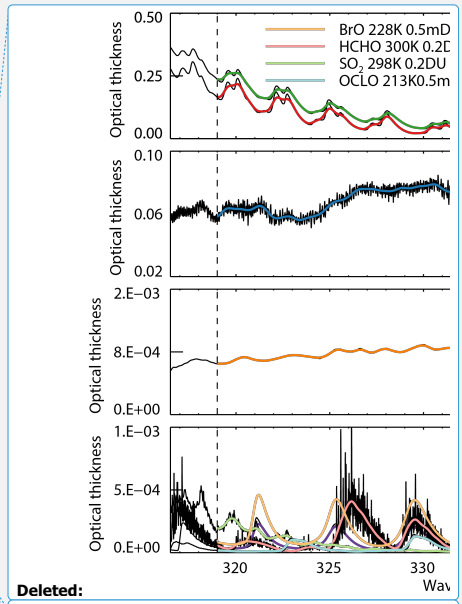

Figure 1. Cross sections used in the current operational BrO algorithm except for the SO_2 cross section at 298 K which is to be used in the next version. The black lines are the original cross sections, the color lines show the cross sections convolved with OMI slit function (which is assumed to be a Gaussian with 0.42nm full width at half maximum. The BrO cross section after multiplication with the wavelength-dependent AMFs used these parameters for the AMF calculation: albedo = 0.05, SZA = 5.0°, and VZA = 2.5°).

Deleted:
Deleted:
Formatted: Font:Not Bold, Complex Script Font: Not Bold
Formatted: Caption, Centered
Deleted:
Deleted: solar zenith angle
Deleted: viewing zenith angle

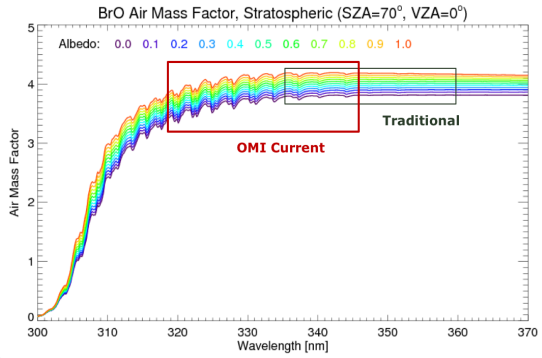

Deleted: ... [1]

Figure 2. Wavelength- and albedo-dependent air mass factors calculated using a mostly stratospheric fixed BrO profile. The blue box shows the fitting window used in our previous versions, and the red box shows the fitting window used in the current operational algorithm.

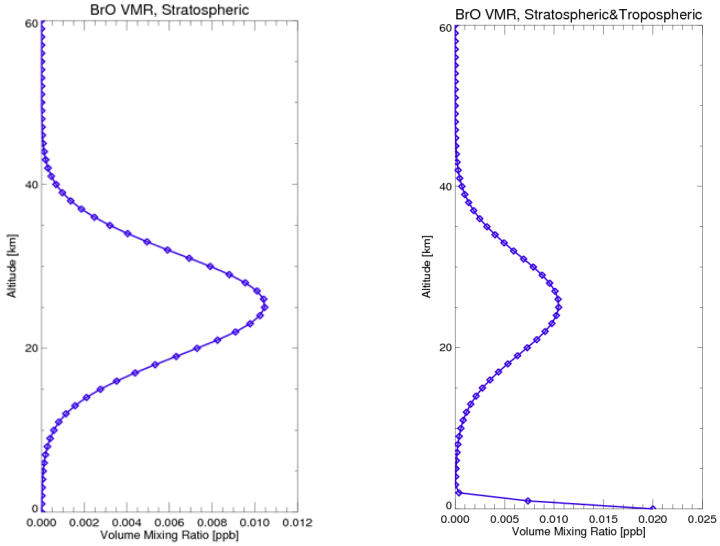

Figure 3. A mostly stratospheric vertical BrO profile used for air mass factors (left panel). Total BrO, BrO < 15 km, BrO < 10 km, and BrO < 5km are 1.55×10^{13}, 5.06×10^{12}, 1.55×10^{12}, and 2.87×10^{11}, respectively. A stratospheric tropospheric vertical BrO profile for air mass factors (right panel) can reduce errors by 50%.

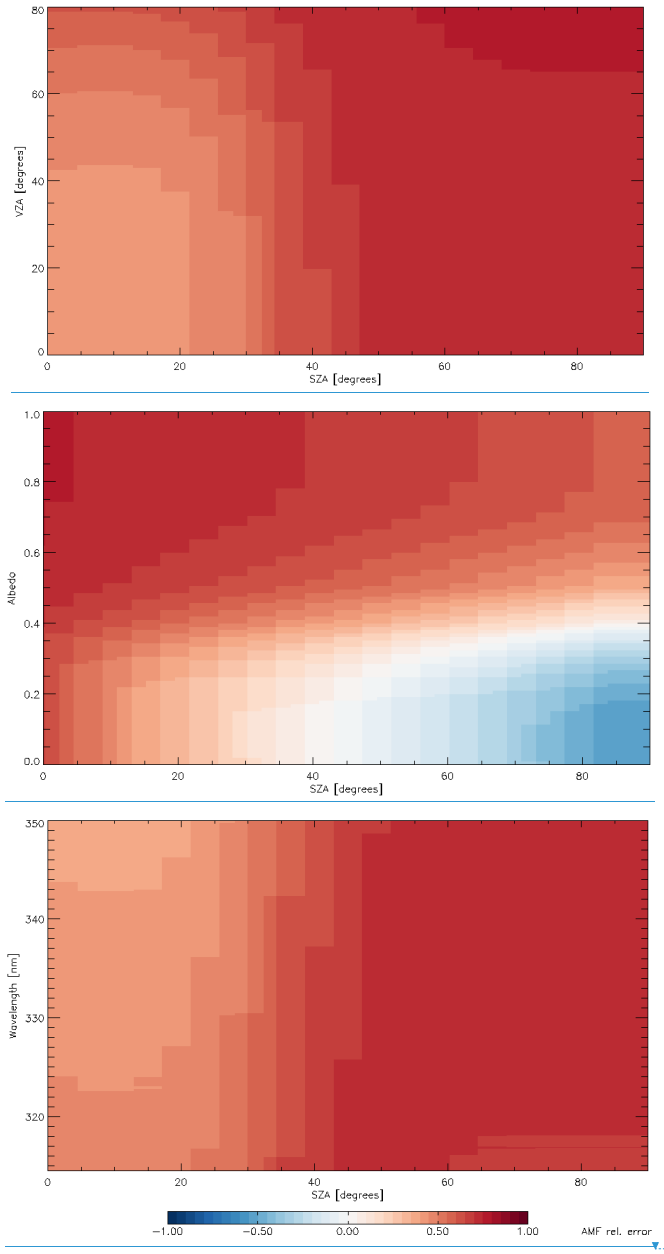

Formatted: Normal, Centered

Deleted:

Figure 4. AMFs relative errors as a function of the SZA and the wavelength (bottom panel), albedo (middle panel) and VZA (top panel).

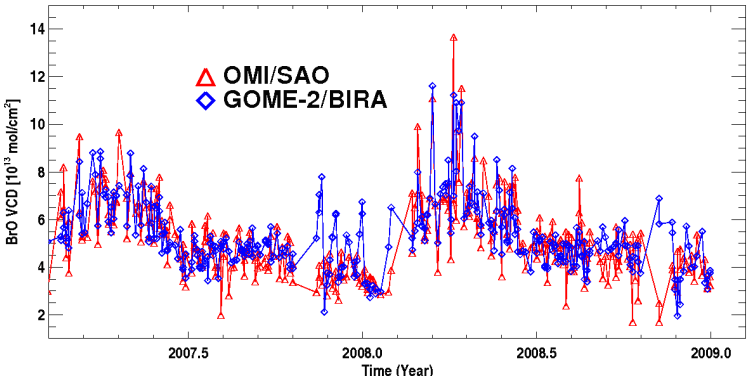

Figure 5. Time series comparison of SAO OMI (red) BrO and BIRA GOME-2 (blue) BrO VCDs from February 2007 to November 2008 using simultaneous nadir overpasses within 2 minutes between OMI and GOME-2 observations.

Deleted:

Formatted: Font color: R,G,B (21,37,192), Complex Script Font: Bold, English (UK)

Deleted: 4

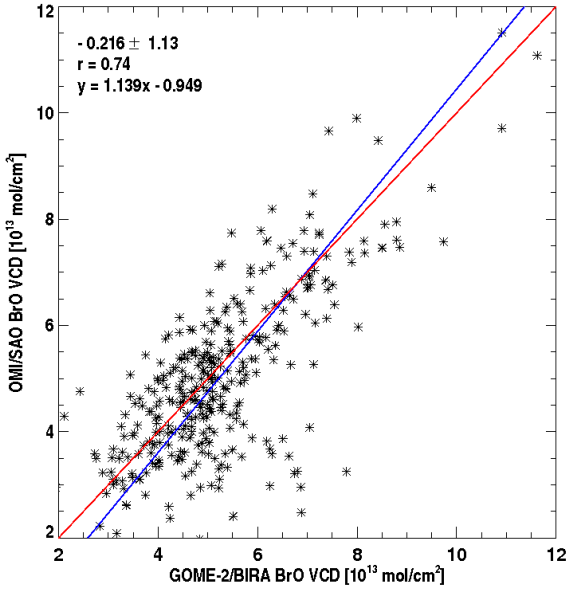

Figure 6. Correlation and orthogonal regression of OMI and GOME-2 BrO for the data shown in Fig. 5. The legends show the mean bias and standard deviation of the differences, correlation, and the orthogonal regression.

Deleted: 5

Deleted: 4

5

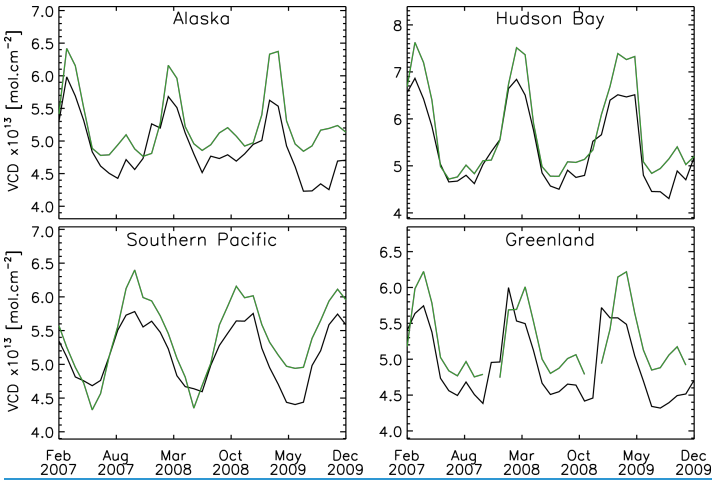

Figure 7. VCD of GOME2 (green) comparison to OMI (black) over four regions from February 2007 to December 2009 for four regions.

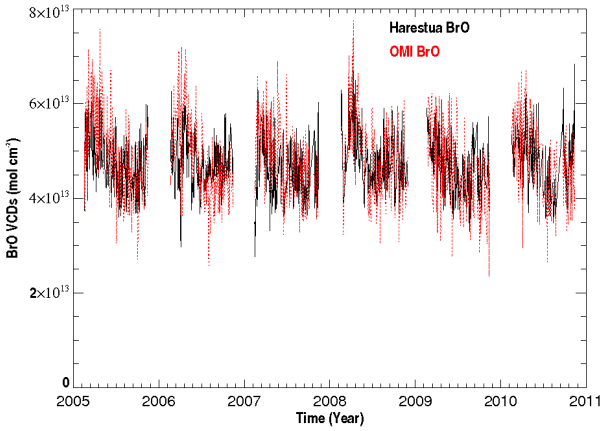

Figure 8. Time series comparison of ground-based zenith-sky total BrO (black) at Harestua, Norway and coincident SAO OMI BrO (red) from February 2005 through August 2011.

Deleted: 6

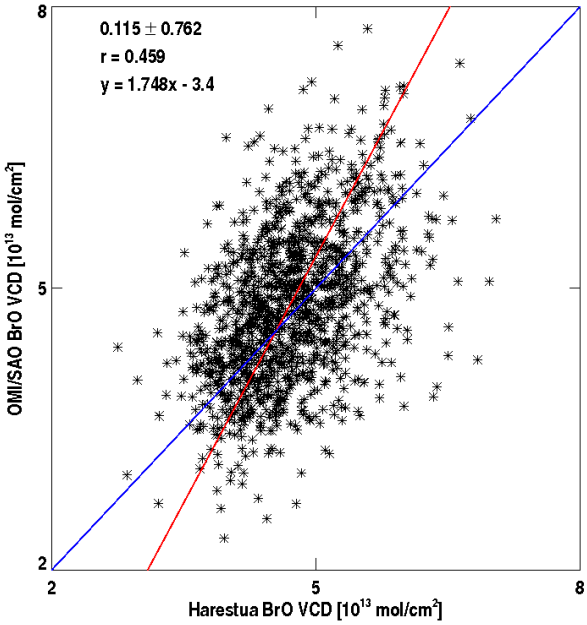

Figure 9. Correlation and orthogonal regression of OMI and Harestua BrO for the data in Fig. 8. The legends show the mean biases and standard deviations of the differences, correlation, and the orthogonal regression.

Deleted: 7

Deleted: 6

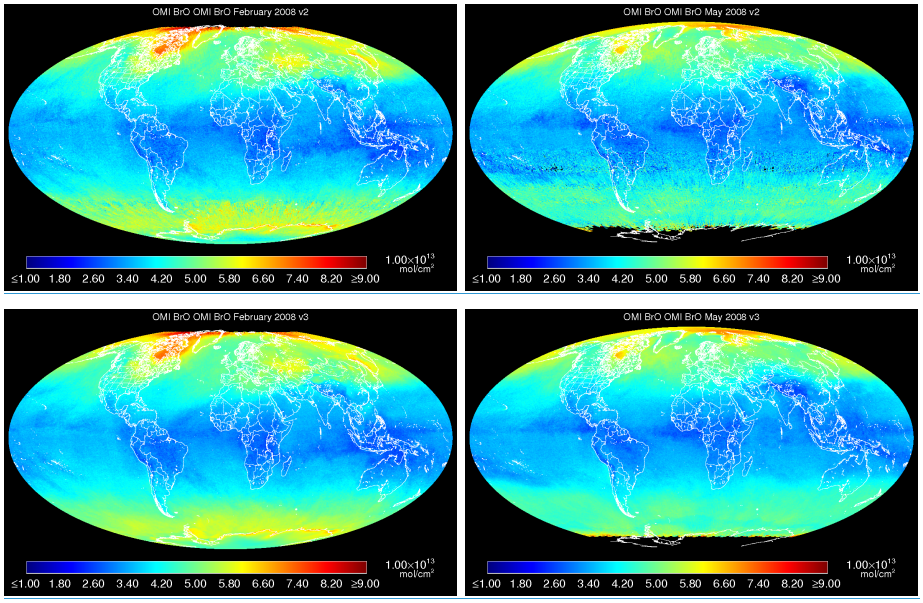

Figure 10. Monthly averages for February and May 2008 for version 3 and version 2.

Formatted: English (UK)

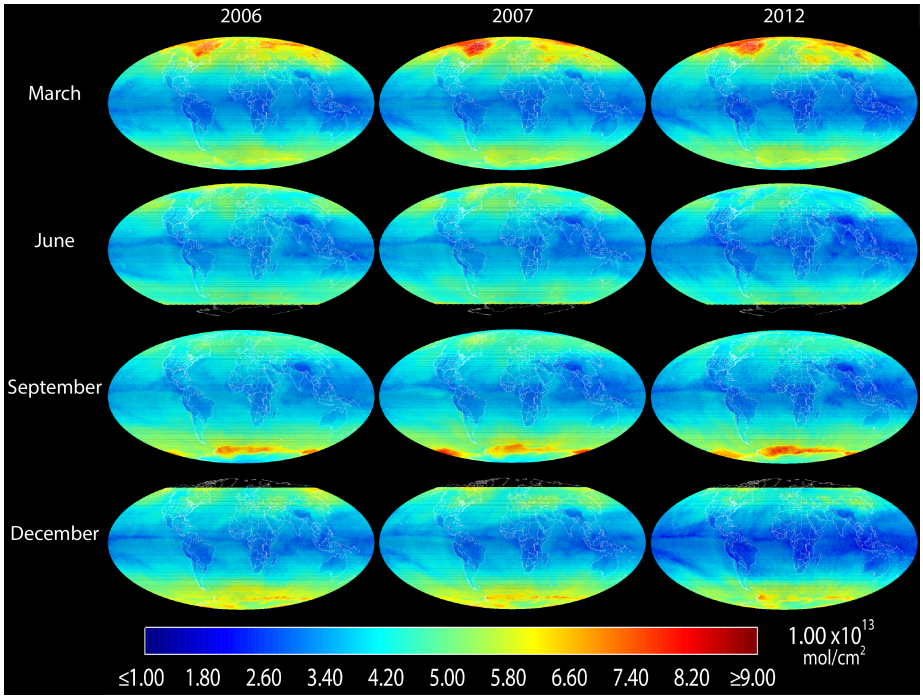

Figure 11, Global distributions of monthly mean BrO VCDs in March, June, September and December (in different rows) of 2006, 2007, and 2012 (different columns). Bromine release "explosions" during the Polar Spring months can be seen clearly.

Deleted: 8

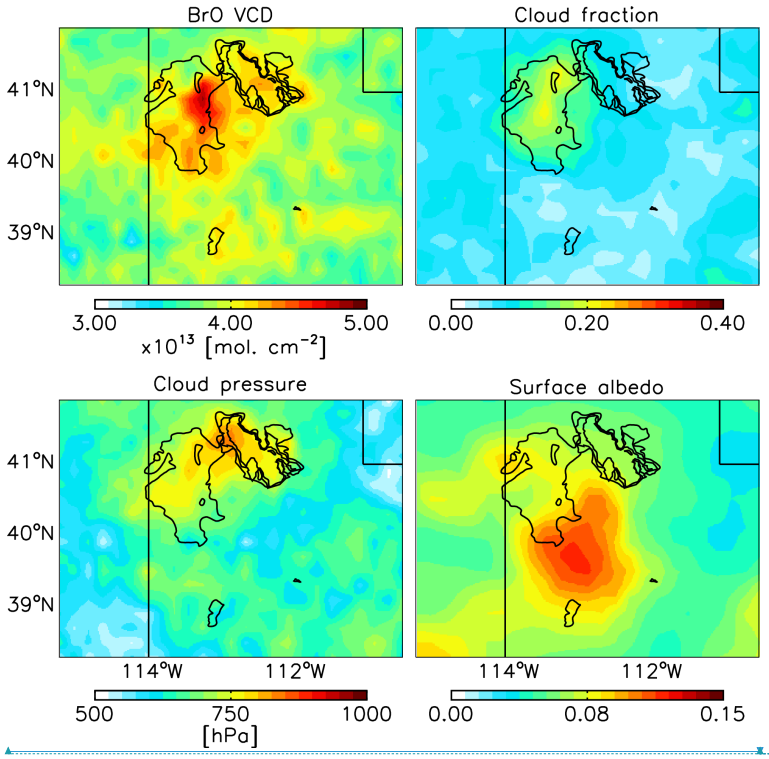

Figure 12. Mean June 2006 BrO VCD over the Great Salt Lake area. Averages have been calculated on a 0.2 x 0.2 degree grid including only pixels with cloud fractions smaller than 0.4.

Formatted: Font color: Accent 1

Formatted: Font:Bold

Formatted: Centered

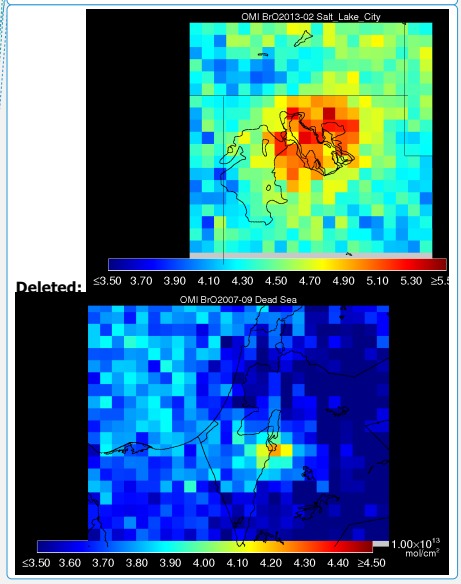

Deleted:

Deleted: 9

Deleted: Monthly mean BrO VCD (left) over the U.S. Great Salt Lake for February 2013 and (right) over the Dead Sea Valley for September 2007.

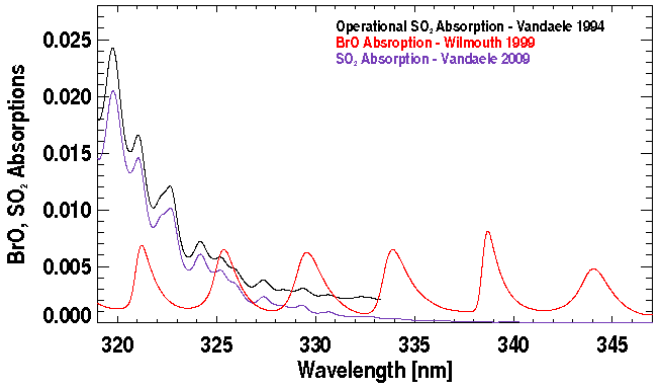

Figure 13. Comparison of BrO absorption (red) and SO_2 absorptions under volcanic scenarios based on cross sections used in the operational algorithm (Vandaele et al., 1994) as shown in black and the recent laboratory cross sections (Vandaele et al., 2009) as shown in purple. For BrO, a SCD of 1.0×10^{14} molecules cm^{-2} is assumed; for SO_2, a SCD of 15 Dobson Units (i.e., 4.03×10^{17} molecules cm^{-2}) is assumed. Cross sections have been convolved with OMI slit function (which is assumed to be a Gaussian with 0.42nm full width at half maximum).

Deleted: 0

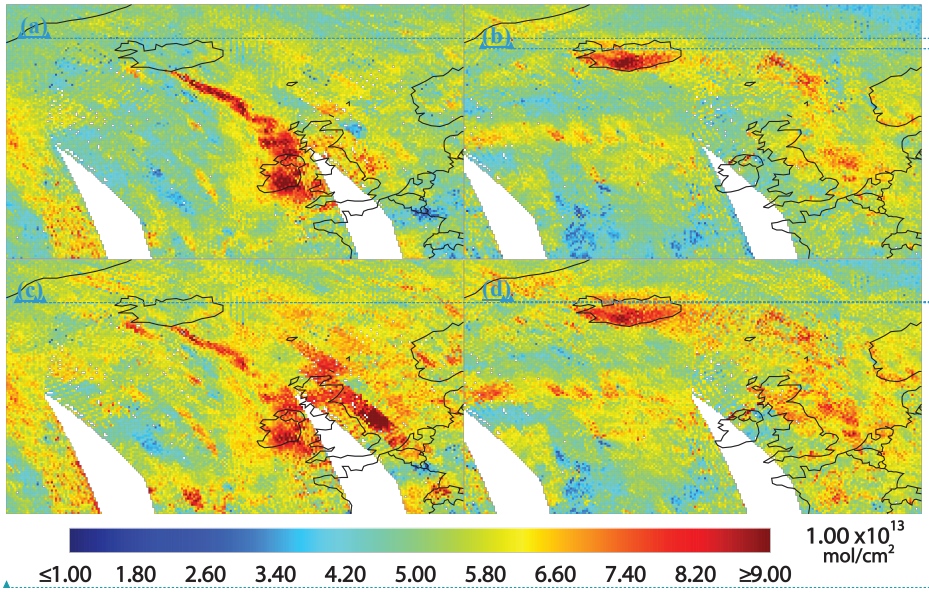

Figure 14. Daily average BrO VCDs from Eyjafjallajökull on May 5 (a) and 17 (b), 2010 produced using the operational SO_2 cross sections and for the same days (c) and (d) using the Vandaele et al. (2009) SO_2 cross sections.

Formatted: Font:Bold
Formatted: Font:Bold, Complex Script Font: Bold
Formatted: Font:Bold, Complex Script Font: Bold, English (US)
Formatted: Font:Bold, Complex Script Font: Bold
Formatted: Font:Bold, Complex Script Font: Bold, English (US)
Formatted: Font:Bold, Complex Script Font: Bold
Formatted: Font:Bold, Complex Script Font: Bold, English (US)
Formatted: Font:Bold, Complex Script Font: Bold
Formatted: Font:Bold, Complex Script Font: Bold
Formatted: Font:Bold, Complex Script Font: Bold, English (US)
Deleted: 1
Deleted: (top)
Deleted: (bottom)

Page 37: [1] Deleted	Raid M Suleiman	1/19/19 2:06:00 PM